haematologica
Journal of the Ferrata Storti Foundation

ATRA resistance conferred by a clustered subset of hotspot PML::RARA mutations enhancing basal repression rather than precluding transactivation

by Glauce M. Barbosa, Hao Yuan, Izabella Tambones, Roland H. Stote, Hsin Chieh Wu, Hugues de Thé, Albane le Maire and Marie-Claude Geoffroy

Received: November 25, 2025.
Accepted: July 31, 2026.

Citation: Glauce M. Barbosa, Hao Yuan, Izabella Tambones, Roland H. Stote, Hsin Chieh Wu, Hugues de Thé, Albane le Maire and Marie-Claude Geoffroy. ATRA resistance conferred by a clustered subset of hotspot PML::RARA mutations enhancing basal repression rather than precluding transactivation. Haematologica. 2026 Aug 13. doi: 10.3324/haematol.2025.300279 [Epub ahead of print]

ATRA resistance conferred by a clustered subset of hotspot PML::RARA mutations enhancing basal repression rather than precluding transactivation

Glauce M. Barbosa[1,*], Hao Yuan[2,3,*], Izabella Tambones[1], Roland H. Stote[4], Hsin Chieh Wu[5] Hugues de Thé[2,3,5,6,#], Albane le Maire[1,#], Marie-Claude Geoffroy[2,5,#]

[1] Université de Montpellier, Centre de Biologie Structurale (CBS), CNRS UMR5048-INSERM U1054, Montpellier, France.

[2] Université Paris Cité, Institut de Recherche Saint-Louis (IRSL), INSERM UMR1342-CNRS EMR8000, Paris, France

[3] Sino-French Research Center for Life Sciences and Genomics, State Key Laboratory of Medical Genomics, CNRS-LIA124, Rui-Jin Hospital, Shanghai Jiao Tong University School of Medicine, Shanghai, China

[4] Université de Strasbourg, IGBMC, CNRS, Inserm, UMR 7104-UMR-S 1258, F-67400 Illkirch, France

[5] Collège de France, Oncologie Cellulaire et Moléculaire, Université Paris Cité, INSERM UMR 1050, CNRS UMR 7241, Paris France

[6]Laboratoire d'hématologie, Hôpital Saint-Louis, Assistance Publique Hôpitaux de Paris (AH/HP), Paris, France

[*] These authors contributed equally to this work.

CORRESPONDENCE

M.C. Geoffroy : marie-claude.geoffroy@inserm.fr, A. le Maire : albane.lemaire@cbs.cnrs.fr, H. de Thé : hugues.dethe@inserm.fr

AUTHOR CONTRIBUTIONS

HdT, AlM and MCG supervised the research. GB, YH, AlM and MCG performed and analysed cellular and biochemical experiments. IT and RS performed molecular dynamic simulations. HCW performed fishing pull-down experiments. MCG, AlM and HdT wrote the manuscript and all co-authors critically reviewed and approved the final manuscript.

ACKNOWLEDGMENTS

We thank Pierre Germain (CBS, Montpellier, France) for assistance with mammalian two-hybrid experiments, Scott Kogan (UCSF, San Francisco, USA) for the gift of the rabbit polyclonal anti-RARA antibody, Henrich Gronemeyer (IGBMC, Strasbourg, France) for providing MEF $RAR^{-/-}$ cell line, William Bourguet (CBS, Montpellier, France) and Dinos Moras (IGBMC, Strasbourg, France) for helpful discussions.

Data Sharing Statement

The data generated in this study are available upon reasonable request from the corresponding authors.

FUNDING

This work was supported by the Institut National du Cancer (INCa) through the PLBIO program (grant PLBIO22-174), the ERC (RARA-AML), Ligue Nationale Contre le Cancer. The animal facility, was supported in part by ANR, through the France 2030 program, ANR-23-IAHU-0005, Paris St. Louis Leukemia Institute. I.T. was supported by the ANR [grant ANR-21-CE11-005-01]. This work was granted access to the HPC resources of IDRIS under the allocation 2025-A0130401234 made by GENCI (Grand Équipement National de Calcul Intensif).

COMPETING INTERESTS

The authors declare no competing financial interests.

RUNNING TITLE

RARα LBD Mutations Drive ATRA Resistance in APL

WORD COUNT

Abstract: 130 words; Main text: 4186 words

Four Figures

Eight Supplementary Figures and three Supplementary Tables

ABSTRACT

Most acute promyelocytic leukemia (APL), driven by the PML::RARA fusion, are now cured with targeted therapies combining all-trans retinoic acid (ATRA) and arsenic trioxide. Some patients treated with earlier ATRA/chemotherapy regimen developed resistance associated with mutations that most often preclude PML::RARA ATRA-binding. Here, we characterized a subset of clustered mutations associated with ATRA-resistance, but not predicted to affect ATRA binding. Most mutants indeed retained full ligand responsiveness, but displayed a basal super-repressive phenotype which did not result from an increased affinity for known corepressors such as NCoR and SMRT. Our findings suggest these mutations are gain-of-function associated with enhanced interactions with unidentified RARA partners with repressive ability. Similar to ATRA-resistant PLZF::RARA variants, these observations stress the role of persistent transcriptional repression of some retinoic acid target genes in acquired ATRA-resistance.

INTRODUCTION

Acute promyelocytic leukemia (APL) is a rare subtype of acute myeloid leukemia (AML) driven by PML::RARA. This is now the most curable AML when targeted therapies combining All-Trans Retinoic Acid (ATRA) and arsenic trioxide (ATO) are used for newly diagnosed patients[1, 2]. When APL patients were receiving first line ATRA/chemotherapy (CT), a third of them relapsed and often became ATRA-resistant[3, 4, 5]. In contrast to recurrent alterations of FLT3, WT1, NRAS and KRAS, which may be found at diagnosis (and even more so at relapse), *de novo* mutations in the RARA moiety of PML::RARA were only associated with relapses[6, 7]. Such ATRA resistance was primarily assigned to mutations in PML::RARA impeding ATRA binding[3, 4, 5, 8].

RARA is a strong basal transcriptional repressor through constitutive interactions with corepressor complexes nucleated by the nuclear receptor corepressor (NCoR)[9,10] or the silencing mediator for retinoid acid and thyroid hormone receptors (SMRT)[11]. Corepressors interact with NRs through their NR interaction domain (NRID), a large disordered region that contains two or three conserved interaction domains (ID1-ID3). Each of them contains NR-binding motifs, known as CoRNR1, CoRNR2 and CoRNR3[12-15]. The molecular mechanisms underlying RARA-mediated repression has been clarified through the crystal structure of the RARA LBD[16] showing that corepressor binding induces a conformational change in RARA's helix H11, converting it into a β-strand (S3), which forms an antiparallel β-sheet with the N-terminal β-strand of the CoRNR1 peptide. Upon agonist binding, this β-strand S3 reverts to the α-helix H11, leading to corepressor release and repositioning of helix H12, thereby facilitating the recruitment of coactivators[17, 18].

Here, we show that some clustered hotspot RARA LBD mutations found in ATRA-resistant APL patients actually trigger basal super-repression, but retain full ligand-responsiveness. Such super-repressive phenotype does not result from enhanced canonical LBD/corepressor binding. Rather, we suggest that they are gain of function mutations driving enhanced binding of non-canonical repressors which drive ATRA-resistance.

METHODS

Plasmid constructs and cell lines

RARA and PML::RARA R1 mutants were generated by site-directed mutagenesis with plasmids and primers listed in *Supplementary Methods.* Cell lines (HEK293T, Plat-E and COS-7) and immortalized MEF RARs$^{-/-}$ were grown and transfected as described in *Supplementary Methods.*

Colony-forming cell assay

Mouse hematopoietic Lin$^-$ progenitors were retrovirally transduced with RARA and PML::RARA R1 mutants to perform colony forming cell assay in methylcellulose supplemented with appropriate cytokines. All procedures were performed with respects of the ethical rules of France. ATRA-induced cell differentiation was then revealed by May-Grünwald Giemsa staining as detailed in *Supplementary methods.*

Western blot analysis

ATRA-induced RARA degradation was monitored in HEK293T cells by SDS-PAGE and immunoblotting techniques described in *Supplementary Methods.*

Transcriptional activities of RARA and PML::RARA R1 mutants

Luciferase reporter assays were performed in HEK293T cells as previously described[19]. Cells were co-transfected with the p3xDR5-TK-Fluc reporter, pTK-RLuc normalization plasmid and pSG5 constructs expressing RARA or PML::RARA R1 mutants. Cells were maintained in charcoal-stripped serum, prior to transfection. Firefly and Renilla luciferase activities were measured 36 hours later using a dual-luciferase reporter kit (Promega).

Gene expression analysis

RNA isolation and cDNA analysis performed with RARA or PML::RARA expressing cells are described in *Supplementary Methods*. For microarray analysis, gene transcripts from immortalized-RARA Lin progenitors were prepared using GeneChip Plus Reagent Kit

(ThermoFisher Scientific). Each sample was hybridized on GeneChip® Mouse transcriptome array 1.0 with the Affymetrix® Fluidics Station 450 (ThermoFisher Scientific). The normalized expression value for each array was calculated using the Affymetrix®software as described in *Supplementary Methods.*

Interaction of RARA LBD mutants with corepressors

Mammalian two-hybrid assays were performed using plasmids containing Gal-DBD coupled to NCoR and SMRT interaction domains, VP16 linked to RARA LBDs, and the $(17m)_{5x}$-G-Luc reporter gene in COS-7 cells as described in *Supplementary Methods.*

Ligand binding affinity and structural modeling

Purification of recombinant RARA LBDs: The proteins were purified as previously described[16]. Structural integrity of all proteins was validated by circular dichroism and dynamic light scattering (Supplementary Figures S4C-D) as detailed in *Supplementary Methods.*

Thermal shift assay (TSA): RARA LBDs stability was assessed by SYPRO orange-based TSA in a qPCR thermocycler. Protein-ligand mixtures were heated from 25-95 °C, and Tm values were derived from fluorescence curves, as described in *Supplementary Methods.*

Steady-state fluorescence anisotropy: Binding assays were performed with fluorescent peptides (Table S3) as previously described[16]. Protein dilutions were mixed with 4 nM labeled peptide ± ligand, and anisotropy was recorded on a Safire microplate reader. Kd values were obtained by nonlinear regression as detailed in *Supplementary Methods*.

Structural modeling: RARA LBD was modeled in its repressive conformation using Alphafold 3.0[20] and molecular dynamics simulation was performed to reveal structural assembly of ATRA-resistant mutants as described in *Supplementary Methods*.

Statistical analysis

Statistical analysis was performed using GraphPad Prism software (V10.6.10). Data from biological or technical replicates were expressed as mean ± standard deviation (SD).

Differences between groups were compared using a two-tailed, unpaired Student's t-test with Welch's correction.

RESULTS

Molecular alterations of RARA ligand-binding domain (LBD) in therapy-resistant APL patients

Genomic analysis of relapsed APL patients revealed that clinical resistance to ATRA was associated with the acquisition of *de novo* mutations in the *RARA* moiety of *PML::RARA* gene (Table S1). More than thirty missense mutations and rare frameshift insertions/deletions (indel) have been reported into three clusters (R1, R2, R3) of RARA LBD (Figure 1A and Supplementary Figure S1A). Many of them are clustered into the R2 region where the ATRA binding pocket assembles (Supplementary Figure S1B). Other hotspot mutations of the R3 region perturb the binding of canonical transcriptional coregulators, while those from the R1 region remain to be explored. Interestingly, RARA LBD mutations were also reported in *de novo* breast fibroepithelial cancer (BFT) in patients never exposed to exogenous retinoids[21, 22]. Remarkably, many RARA mutations were quite similar in both diseases, with over half of the mutations identical in the R2 region (Supplementary Figure S1A-B). However, the R1 region was much less prone to mutation in BFT patients, when compared to APL, with only 3 residues (L224P, W225C/R and C235F) overlapping (Supplementary Figure S1A).

To explore clustered PML::RARA R1 mutations, we focused on five (Y208N, R217H, L224P, C235Y, and K238E) of them (Figure 1A and Supplementary Figure S2A). These mutations are located in the loop between H2 and H3 or within helix H3, generally without direct orientation toward the ligand binding pocket (LBP), nor toward the coregulator binding site (Figure 1B), prompting the functional evaluation on RARA transcriptional activities.

RARA and PML::RARA R1 mutants exhibit distinct ATRA-sensitivity of clonogenic activity

Enforced RARA or PML::RARA expression can confer self-renewal onto primary

hematopoietic progenitors[8, 23, 24]. We first examined whether R1 mutations (Y208N, R217H, L224P, C235Y or K238E) may alter clonogenic activity of RARA and PML::RARA (Figure 1C). While Lin$^-$ progenitors transduced with an empty vector quickly stop to grow after the second replating, RARA or PML::RARA overexpression conferred extended self-renewal, allowing continued clonogenic activity (Figure 1D, Supplementary Figure S2B and C). Importantly, RARA or PML::RARA wild-type (WT) and mutants all behaved similarly, indicating that mutations of the R1 region do not affect progenitor immortalization (Figure 1D and G, Supplementary Figure S2C).

We then analysed the clonogenic activity of RARA and PML::RARA-immortalized progenitors in the presence of 100 nM ATRA, starting at the second replating. Upon retinoid exposure, colonies number drastically reduced in both WT RARA and PML::RARA and to a lesser extent for Y208N, R217H, and K238E, while L224P and C235Y were unaffected (Figure 1E, F and G, Supplementary Figure S2D). Cell morphology before and after ATRA treatment by May-Grünwald Giemsa (MGG) staining confirmed the lack of differentiation in RARA or PML::RARA L224P and C235Y immortalized cells, as opposed to WT or the other RARA mutants (Figure 1H and I). Critically, when ATRA-treated differentiated cells were replated in ATRA-containing media, a significant residual clonogenic activity consistently remained for the Y208N, R217H and K238E mutants for either RARA or PML::RARA (Figure 1E and F, Supplementary Figure S2D). Thus, despite massive ATRA-induced differentiation, progenitors immortalized by RARA or PML::RARA R1 cluster mutants retain a significant clonogenic activity in ATRA presence, sharply contrasting with WT.

We also monitored the ATRA-induced degradation of RARA and PML::RARA in transfected HEK293T cells by Western blot analysis (Supplementary Figure S2E and F). As expected, L224P and C235Y were not degraded upon ATRA treatment, suggesting that they fail to respond to ATRA, as opposed to WT or other RARA and PML::RARA mutants.

Differential transcriptional activities of RARA and PML::RARA R1 mutants

To assess whether mutations in the R1 cluster may affect transcriptional activities of

RARA and PML::RARA, we performed a dual-luciferase reporter assay in HEK293T cells with a sensitive ATRA-responsive reporter[19] (Figure 2A and B, Supplementary Figure S3A). Remarkably, this assay revealed that all RARA R1 mutants exhibit a much stronger basal repression activity compared to WT (Figure 2B). Upon addition of 100 nM ATRA, RARA mutants displayed full transcriptional activities, except for L224P and to a lesser extent C235Y, which likely exert a dominant negative activity on endogenous RARs. Due to their location on RARA LBD, these mutations are not expected to substantially impact DNA binding and heterodimerization, allowing efficient transactivation. The same conclusions can be drawn for PML::RARA R1 mutants, although PML::RARA acts as a much stronger basal repressor and remains less responsive to ATRA induction (Supplementary Figure S3A), likely reflecting PML-enhanced repression[23, 25].

To bypass the basal activity of endogenous RARs, we analysed transcriptional activities of RARA and PML::RARA mutants stably expressed in mouse embryonic fibroblast where all three RAR genes were functionally inactivated (MEF RARs$^{-/-}$)[26] and analysed gene expression of three ATRA-responsive genes (*Cyp26a1and Rarb* for RARA and *Cyp26b1* for PML::RARA)[27-29]. After 12h ATRA exposure, Y208N, R217H and K238E mutants induced robust expression of *CYP26A1* or *RARB* comparable to WT RARA, while L224P did not and C235Y exhibited a blunted activation profile (Figure 2C and D). Critically, a significant basal repression of *RARB* gene was again observed for all mutants. For WT and PML::RARA R1 mutants, similar results were obtained with *Cyp26b1,* another gene involved retinoic acid clearance (supplementary Figure S3B and C).

We then examined by microarray analysis the basal and RA-responsive transcriptional profiles of canonical RA-responsive genes (*CYP26A1, DHRS3, NRIP1)* in RARA-immortalized Lin$^-$ progenitors (Figure 2E). Again, in the absence of added ATRA, RARA mutants behave as super repressors, while upon addition of RA, these target genes were reactivated, except by L224P. Collectively, while two mutants (L224P and C235Y) are insensitive (or poorly sensitive) to ATRA, similar to those from the R2 cluster, the three other R1 mutants exhibit enhanced basal repression, but remain capable to fully activate transcription and initiate differentiation.

Altogether, RARA and PML::RARA mutants share similar phenotypes in terms of clonogenicity, ATRA-induced cell differentiation and transcriptional activation upon retinoid treatment. Biophysical studies were thus performed on RARA to further understand ATRA-resistance of PML::RARA mutants.

L224P and C235Y mutants exhibit impaired retinoid binding

To biochemically explore ATRA binding affinity of these mutants, we analysed the stability of all mutants, with or without ligand, using thermal shift assay (TSA) (Figure 3A). The purified recombinant RARA LBD proteins (Supplementary Figure S4A) were incubated with either AM580, a synthetic RARA agonist, more stable than ATRA, or BMS493, a pan-RARA inverse agonist[30]. The proteins were then subjected to a thermal gradient, and the fluorescent signal of an external dye, which binds to exposed hydrophobic residues during protein denaturation, was monitored (Figure 3B, Supplementary Figure S4B). In the presence of increasing ligand concentration, Y208N, R217H, and K238E exhibited significant ligand-induced protein stabilization comparable to WT RARA LBD. In contrast, the thermal stability of L224P and C235Y mutants remained essentially unchanged with and without ligand incubation, again suggestive for a low ligand binding affinity.

To further investigate the defective ligand binding of L224P and C235Y, we performed structural modelling of these LBD variants using AlphaFold 3.0 models[20] (Figure 3C). The L224P mutation is predicted to induce a local helix-to-coil transition, in agreement with the reduced α-helical content observed in circular dichroism (CD) (Supplementary Figure S4C). Molecular dynamics simulations showed an increased flexibility of the H2-H3 loop in L224P (Supplementary Figure S4E), along with the loss of stabilizing hydrophobic interactions between L224 and residues T210 and N212 (Figure 3C, Supplementary Figure S4F-G). In addition, the proline substitution allows a CH / π interaction with F286, preventing ligand binding (Supplementary Figure S4H). On the other hand, the C235Y mutation introduces a bulky side chain into the LBP (Figure 3C). DoGSite3 calculations reveal a smaller and shallower mutant pocket compared to the wild-type, with reduced volume (428.03 $Å^3$ and

523.26 Å^3, respectively) and surface area (295.88 Å^2 and 465.98 Å^2), likely causing steric hindrance that interferes with ligand binding.

Luciferase reporter assays on WT and RARA R1 mutants comparing increasing concentrations of ATRA or AM580 confirmed reduced L224P and C235Y activation by both ligands (Supplementary Figure S5). Rigid molecular docking analyses using AutoDock4 of AM580 and ATRA on the C235Y RAR model indicated that AM580 is unable to enter the LBP (Supplementary Figure S6A). Although ATRA could be accommodated within the LBP in a subset of docking poses, it adopts a titled, non-favourable conformation that fails to preserve the canonical interactions with RARA previously described in crystallographic structures[31,32] (Supplementary Figure S6B and D). Flexible molecular docking showed some limited contacts between the ligands and the C235Y RARA protein (Supplementary Figure S6C and D) that could be relevant for co-activator recruitment and that could interplay with the observed residual receptor transactivation. These structural insights confirm that the C235Y mutation introduces steric clashes affecting both AM580 and ATRA binding, in agreement with the functional assays performed in the presence of these ligands.

To further understand the differential response of RARA mutants to ATRA (Figure 2B), we next evaluated their interaction with canonical coactivators (SRC-1 and TIF-2) using fluorescence anisotropy experiments (Figure 3D) with NR-box2 (NR2) peptide which presents the highest affinity for RARA solely in the presence of ligands[33] (Figure 3E, Supplementary Figure S7). Critically, most RARA mutants displayed normal ligand-inducible interactions, while, as expected, L224P demonstrated a strongly altered ATRA

RARA mutants do not exhibit a strong basal increase of classical corepressor binding

We next assessed the binding affinities of RARA mutants with the two well-characterized SMRT and NCoR corepressors that interact with NRs through specific domains (ID1-ID3) (Figure 4A). We focused on the role of ID1 including the minimal CoRNR1 motif described as the main interaction domain of SMRT and NCoR with RARA[16]. Fluorescence anisotropy experiments using these CoRNR1 peptides confirmed the strongly reduced

interaction with the previously described I396E RARA mutant[16] (Figure 4B and Supplementary Figure S8). These demonstrated that, while all RARA LBD mutants exhibited a stronger affinity for SMRT than for NCoR[16], no significant differences were found when the binding affinities of RARA LBD WT and mutants were compared (Figure 4B and Supplementary Figure S8).

Mammalian two-hybrid assays (Figure 4C) were also performed in the absence of ligand to evaluate the binding affinity of RARA LBD mutants with SMRT and NCoR short NRID version with ID1 intact alone or in combination with a mutant ID2 (ID1+ID2m) that disrupts ID2-mediated interactions[16] (Figure 4A). While the I396E mutant exhibited a strongly reduced affinity for all the corepressors, no significant difference in SMRT ID1+ID2m recruitment was observed for RARA LBD mutants compared to WT RARA LBD (Figure 4D). Altogether, these results suggest that the super-repressive activity observed for RARA mutants (Figure 2A) is not linked to a stronger interaction with canonical corepressors.

DISCUSSION

This study explored mutations in the R1 cluster of RARA and PML::RARA associated with ATRA-resistance in APL. Two of these mutations (L224P and C235Y) abolish or impede ATRA-binding (absence of ligand-induced receptor stabilization, transcriptional activation or proteolysis in both RARA and PML::RARA proteins). These two mutations thus mimic the classic mutations present in the R2 and R3 clusters of ATRA-resistant APL or *de novo* BFT [21, 22]. Remarkably, we also characterized a distinct class of RARA mutations (exemplified by Y208N, R217H, K238E), associated with enhanced basal repression, but preserved ligand-induced transcriptional activation, a phenotype easier to demonstrate in the context of RARA, since PML::RARA exhibits multiple distinct mechanisms of repression[23, 25]. Functionally, these mutations in the context of both RARA and PML::RARA impeded full ATRA-induced loss of clonogenic activity, but did not prevent differentiation *ex vivo*, in contrast to R2, R3 mutations, which are essentially ATRA-insensitive. Despite induction of terminal differentiation, some residual clonogenic activity remained, although the ATRA-treated colonies were clearly smaller in size, again highlighting the incomplete coupling between differentiation and loss of self-

renewal[34]. Moreover, ATRA-treated mutant cells retained the capacity to re-grow for at least two passages, while WT RARA-transformed progenitors failed to do so. This situation closely resembles that of PLZF::RARA-transformed cells, where PLZF provides an additional repression domain which precludes loss of clonogenic growth and clinical response, but not ATRA-induced differentiation or degradation of the fusion protein[35-38]. This suggests that in addition to PML::RARA degradation and subsequent reformation of PML nuclear bodies[38], complete reversal of transcriptional repression is required for efficient loss of self-renewal, while activation/derepression of a distinct set of genes suffice to drive terminal differentiation.

Investigating the origin of the super repression in R1 mutants, our biochemical and biophysical studies do not support enhanced interactions with "classic" corepressors. This is in line with the fact that Y208N, R217H or K238E are all located far from known corepressor-binding surfaces. We therefore propose that these mutations are gain of function, potentially enforcing strong interactions with yet unidentified RARA partners with repressive ability (Figure 4E). Identifying these factors could be an important goal, in view of the renewed interest in RARA and ATRA signalling in others malignancies[39]. Altogether, this study unravels the varied molecular mechanisms that contribute to RA-resistance in APL and draw an unexpected parallel with the well-characterized basis of resistance in PLZF::RARA variants.

REFERENCES

1. Lo-Coco F, Cicconi L, Breccia M. Current standard treatment of adult acute promyelocytic leukaemia. Br J Haematol. 2016;172(6):841-854.

2. Voso MT, Guarnera L, Lehmann S, et al. Acute promyelocytic leukemia: long-term outcomes from the HARMONY project. Blood. 2025;145(2):234-243.

3. Ding W, Li YP, Nobile LM, et al. Leukemic cellular retinoic acid resistance and missense mutations in the PML::RARalpha fusion gene after relapse of acute promyelocytic leukemia from treatment with all-trans retinoic acid and intensive chemotherapy. Blood. 1998;92(4):1172-1183.

4. Gallagher RE, Schachter-Tokarz EL, Zhou DC, et al. Relapse of acute promyelocytic leukemia with PML::RARalpha mutant subclones independent of proximate all-trans retinoic acid selection pressure. Leukemia. 2006;20(4):556-562.

5. Gallagher RE, Moser BK, Racevskis J, et al. Treatment-influenced associations of PML-RARalpha mutations, FLT3 mutations, and additional chromosome abnormalities in relapsed acute promyelocytic leukemia. Blood. 2012;120(10):2098-2108.

6. Madan V, Shyamsunder P, Han L, et al. Comprehensive mutational analysis of primary and relapse acute promyelocytic leukemia. Leukemia. 2016;30(8):1672-1681.

7. Cancer Genome Atlas Research Network, Ley TJ, Miller C, et al. Genomic and epigenomic landscapes of adult de novo acute myeloid leukemia. N Engl J Med. 2013;368(22):2059-2074.

8. Lehmann-Che J, Bally C, Letouze E, et al. Dual origin of relapses in retinoic-acid resistant acute promyelocytic leukemia. Nat Commun. 2018;9(1):2047.

9. Seol W, Mahon MJ, Lee YK, et al. Two receptor interacting domains in the nuclear hormone receptor corepressor RIP13/N-CoR. Mol Endocrinol. 1996;10(12):1646-1655.

10. Zamir I, Harding HP, Atkins GB, et al. A nuclear hormone receptor corepressor mediates transcriptional silencing by receptors with distinct repression domains. Mol Cell Biol. 1996;16(10):5458-5465.

11. Cohen RN, Brzostek S, Kim B, et al. The specificity of interactions between nuclear hormone receptors and corepressors is mediated by distinct amino acid sequences within the interacting domains. Mol Endocrinol. 2001;15(7):1049-1061.

12. Hu X, Lazar MA. The CoRNR motif controls the recruitment of corepressors by nuclear hormone receptors. Nature. 1999;402(6757):93-96.

13. Hu X, Li Y, Lazar MA. Determinants of CoRNR-dependent repression complex assembly on nuclear hormone receptors. Mol Cell Biol. 2001;21(5):1747-1758.

14. Perissi V, Staszewski LM, McInerney EM, et al. Molecular determinants of nuclear receptor-corepressor interaction. Genes Dev. 1999;13(24):3198-3208.

15. Nagy L, Kao HY, Love JD, et al. Mechanism of corepressor binding and release from nuclear hormone receptors. Genes Dev. 1999;13(24):3209-3216.

16. le Maire A, Teyssier C, Erb C, et al. A unique secondary-structure switch controls constitutive gene repression by retinoic acid receptor. Nat Struct Mol Biol. 2010;17(7):801-807.

17. Onate SA, Tsai SY, Tsai MJ, et al. Sequence and characterization of a coactivator for the steroid hormone receptor superfamily. Science. 1995;270(5240):1354-1357.

18. Voegel JJ, Heine MJ, Zechel C, et al. TIF2, a 160 kDa transcriptional mediator for the ligand-dependent activation function AF-2 of nuclear receptors. EMBO J. 1996;15(14):3667-3675.

19. Liu X, Yuan H, Peres L, et al. The DNA binding property of PML::RARA but not the integrity of PML nuclear bodies is indispensable for leukemic transformation. PLoS One. 2014;9(8):e104906.

20. Abramson J, Adler J, Dunger J, et al. Accurate structure prediction of biomolecular interactions with AlphaFold 3. Nature. 2024;630(8016):493-500.

21. Tan J, Ong CK, Lim WK, et al. Genomic landscapes of breast fibroepithelial tumors. Nat Genet. 2015;47(11):1341-1345.

22. Huang XX, Ng LM, Lee PH, et al. Effects of RARalpha ligand binding domain mutations on breast fibroepithelial tumor function and signaling. NPJ Breast Cancer. 2025;11(1):1.

23. Zhu J, Zhou J, Peres L, et al. A sumoylation site in PML::RARA is essential for leukemic transformation. Cancer Cell. 2005;7(2):143-153.

24. Du C, Redner RL, Cooke MP, et al. Overexpression of wild-type retinoic acid receptor alpha (RARalpha) recapitulates retinoic acid-sensitive transformation of primary myeloid progenitors by acute promyelocytic leukemia RARalpha-fusion genes. Blood. 1999;94(2):793-802.

25. Wu HC, Laplantine E, Esnault E, et al. PML-driven sumoylation of PML::RARA-bound co-repressors drives immortalization of primary hematopoietic progenitors. bioRxiv . 2026 Jan 5. doi: 10.64898/2026.01.05.697641 [preprint, not peer-reviewed].

26. Altucci L, Rossin A, Hirsch O, et al. Rexinoid-triggered differentiation and tumor-selective apoptosis of acute myeloid leukemia by protein kinase A-mediated desubordination of retinoid X receptor. Cancer Res. 2005;65(19):8754-8765.

27. de The H, Vivanco-Ruiz MM, Tiollais P, et al. Identification of a retinoic acid responsive element in the retinoic acid receptor beta gene. Nature. 1990;343(6254):177-180.

28. Loudig O, Maclean GA, Dore NL, et al. Transcriptional co-operativity between distant retinoic acid response elements in regulation of Cyp26A1 inducibility. Biochem J. 2005;392(Pt 1):241-248.

29. Ghiaur G, Yegnasubramanian S, Perkins B, et al. Regulation of human hematopoietic stem cell self-renewal by the microenvironment's control of retinoic acid signaling. Proc Natl Acad Sci U S A. 2013;110(40):16121-16126.

30. le Maire A, Teyssier C, Balaguer P, et al. Regulation of RXR-RAR Heterodimers by RXR- and RAR-Specific Ligands and Their Combinations. Cells. 2019;8(11):1392.

31. Sato Y, Ramalanjaona N, Huet T, et al. The "Phantom Effect" of the Rexinoid LG100754: structural and functional insights. PLoS One. 2010;5(11):e15119.

32. Renaud JP, Rochel N, Ruff M, et al. Crystal structure of the RAR-gamma ligand-binding domain bound to all-trans retinoic acid. Nature. 1995;378(6558):681-689.

33. Senicourt L, le Maire A, Allemand F, et al. Structural Insights into the Interaction of the Intrinsically Disordered Co-activator TIF2 with Retinoic Acid Receptor Heterodimer (RXR/RAR). J Mol Biol. 2021;433(9):166899.

34. de The H. Differentiation therapy revisited. Nat Rev Cancer. 2018;18(2):117-127.

35. Nasr R, Guillemin MC, Ferhi O, et al. Eradication of acute promyelocytic leukemia-initiating cells through PML-RARA degradation. Nat Med. 2008;14(12):1333-1342.

36. Koken MH, Daniel MT, Gianni M, et al. Retinoic acid, but not arsenic trioxide, degrades the PLZF::RARAlpha fusion protein, without inducing terminal differentiation or apoptosis, in a RA-therapy resistant t(11;17)(q23;q21) APL patient. Oncogene. 1999;18(4):1113-1118.

37. Nasr R, de The H. Eradication of acute promyelocytic leukemia-initiating cells by PML::RARA-targeting. Int J Hematol. 2010;91(5):742-747.

38. Ablain J, Leiva M, Peres L, et al. Uncoupling RARA transcriptional activation and degradation clarifies the bases for APL response to therapies. J Exp Med. 2013;210(4):647-653.

39. de Botton S, Cluzeau T, Vigil C, et al. Targeting RARA overexpression with tamibarotene, a potent and selective RARalpha agonist, is a novel approach in AML. Blood Adv. 2023;7(9):1858-1870.

FIGURE LEGENDS

Figure 1: RARA and PML::RARA R1 mutants exhibit distinct ATRA-sensitivity of clonogenic activity. (A) Schematic representation of RARA domain organization (A to F) showing *de novo* mutations identified in RA-resistant APL patients within the R1, R2 and R3 regions of the RARA LBD. The mutations studied in this work are highlighted in red. DBD: DNA binding domain; LBD: Ligand binding domain. **(B)** Positioning of the Y208, R217, L224, C235 and K238 amino acids on the crystal structure of RARA LBD (PDB code 3KMZ or PDB code 3KMR, in complex with either the CoRNR1 peptide of NCoR (blue) and the inverse agonist BMS493 (shown as green sticks) (left scheme) or the NR2 peptide of SRC-1 (green) and the agonist AM580 (shown as blue sticks) (right scheme), respectively (16). Residues are displayed as red spheres and are all located into the loop H2-H3 or within H3 helix as illustrated on the schematic representation of RARA LBD below. **(C)** Schematic of colony-forming cell (CFC) assay of mouse Lin^- hematopoietic progenitors transformed with RARA and grown in methyl-cellulose medium for serial passages. 5-FU: 5-Fluorouracil. **(D)** Colony counts from serial replating of 10^4 cells grown in methylcellulose for three passages (MCI to MCIII). Graph shows means +/- SD of n=3 biological replicates. **** p<0,0001 by two-tailed unpaired t-test with Welch's correction comparing RARA with vector at passage III **(E-F)** Colony counts of RARA and PML::RARA-immortalized cells recovered from MCII and grown in the presence of 100 nM ATRA (1^{st} passage). ATRA-resistant colonies were re-grown with 100 nM ATRA (2^{nd} passage) (means +/- SD of n=3 biological replicates). **(G)** RARA colonies before and after a 1^{st} and 2^{nd} passage with ATRA illustrating their differential sensitivity to the ligand. Scale bar= 200 µm. **(H-I)** MGG staining showing morphological changes of RARA and PML::RARA-immortalized Lin^- progenitors in response to 1 µM ATRA for 3 days. Scale bar= 20 µm. Graphs and images shown in (D to I) are representative of three independent biological experiments.

Figure 2: Transcriptional activity of RARA R1 mutants. (A) Schematic representation of the luciferase reporter assay performed in HEK293T cells with the 3xDR5-Luc reporter **(B).** Graph showing transcriptional activities of RARA mutants with or without 100 nM ATRA for 6h.

Relative luciferase activity corresponds to the ratio of firefly to renilla luciferase signal (means +/- SD of n=3 technical replicates). **(C-D)** RT-qPCR analysis of two ATRA-responsive genes (*CYP26A1* and *RARB*) in MEF RAR$^{-/-}$ cells transduced with RARA mutants and exposed to vehicle or 100 nM ATRA for 12h (means +/- SD of n=3 technical replicates). **(E)** Microarray analysis of immortalized Lin-RARA R1 mutants exposed or not to ATRA for 6h and 12h. Graph shows the expression profile of *Cyp26A1*, *DHRS3* and *NRIP1* genes as log2fold change relative to WT. Graphs C and D are representative of three independent biological experiments. Statistical significance assessed by two-tailed unpaired t-tests with Welch's correction comparing RARA R1 mutants with WT (**** p<0,0001, *** p<0,001, ** p<0,01).

Figure 3: Agonist and coactivator binding to RARA LBD mutants. (A) Principle of Thermal Shift Assay (TSA) to assess retinoid binding to recombinant RARA LBD by measuring ligand-induced stabilization of the protein during thermal unfolding. **(B)** Melting temperature of WT and RARA R1 mutants measured by TSA in the presence of increasing AM580 concentrations. Columns from left to right represent protein-ligand ratios: 1:0; 1:0.25; 1:0.5; 1:1; and 1:2. Graph shows means +/- SD of n=3 independent biological replicates (p**** p<0,0001, *** p<0,001, ** p<0,001, ns, not significant) by a two-tailed unpaired t-test with Welch's correction comparing untreated sample with each RARA at a 1:2 protein ligand ratio. **(C)** Zoom in the crystal structure of RARA LBD (PDB code 3KMR) showing L224 and C235, as blue and green sticks, respectively whereas the mutated residues, P224 and Y235, are represented with yellow and pink sticks, respectively. Residues T210 and N212 involved in hydrophobic interactions with L224 are displayed in grey, as well as the synthetic AM580 ligand displayed in orange. **(D)** Principle of steady-state fluorescence anisotropy experiment and description of the peptides derived from SRC-1 and TIF-2, to measure coactivator binding to RARA LBD. **(E)** Dissociation constants (Kd) deduced from fluorescence anisotropy experiments performed for RARA LBD WT and mutants using coactivator peptides, in the presence of AM580. Graph shows means +/- SD of n=3 independent biological replicates (p** <0,001, p* <0,01 by a two-tailed unpaired t-test with Welch's correction comparing L224P with WT).

Figure 4: Corepressor binding to RARA LBD mutants. (A) Schematic of SMRT and NCoR peptides and constructs used in fluorescence anisotropy experiments and mammalian two-hybrid assays. **(B)** Dissociation constants (Kd) deduced from fluorescence anisotropy experiments performed in the absence of ligand for RARA LBD WT and mutants using CoRNR1 peptides from NCoR and SMRT. Graph shows means +/- SD of n=3 independent biological replicates (p** <0,001, p* <0,01 by a two-tailed unpaired t-test with Welch's correction comparing I396E with WT. **(C)** Principle of the mammalian two hybrid assays. UAS: Upstream activation sequence. **(D)** Mammalian two-hybrid assays in COS-7 cells to assess the interaction of RARA LBD mutants with SMRT and NCoR constructs. Graph shows luciferase activities (means +/- SD of n=3 independent biological replicates). **(E)** Interaction model of RARA with corepressors (NCoR and SMRT) in the context of RXR heterodimer, in physiological and pathological conditions, (I. WT) and (II. RARA R1 mutants), respectively. Hypothetical additional corepressors involved in the interaction with RARA mutants are shown as orange spheres.

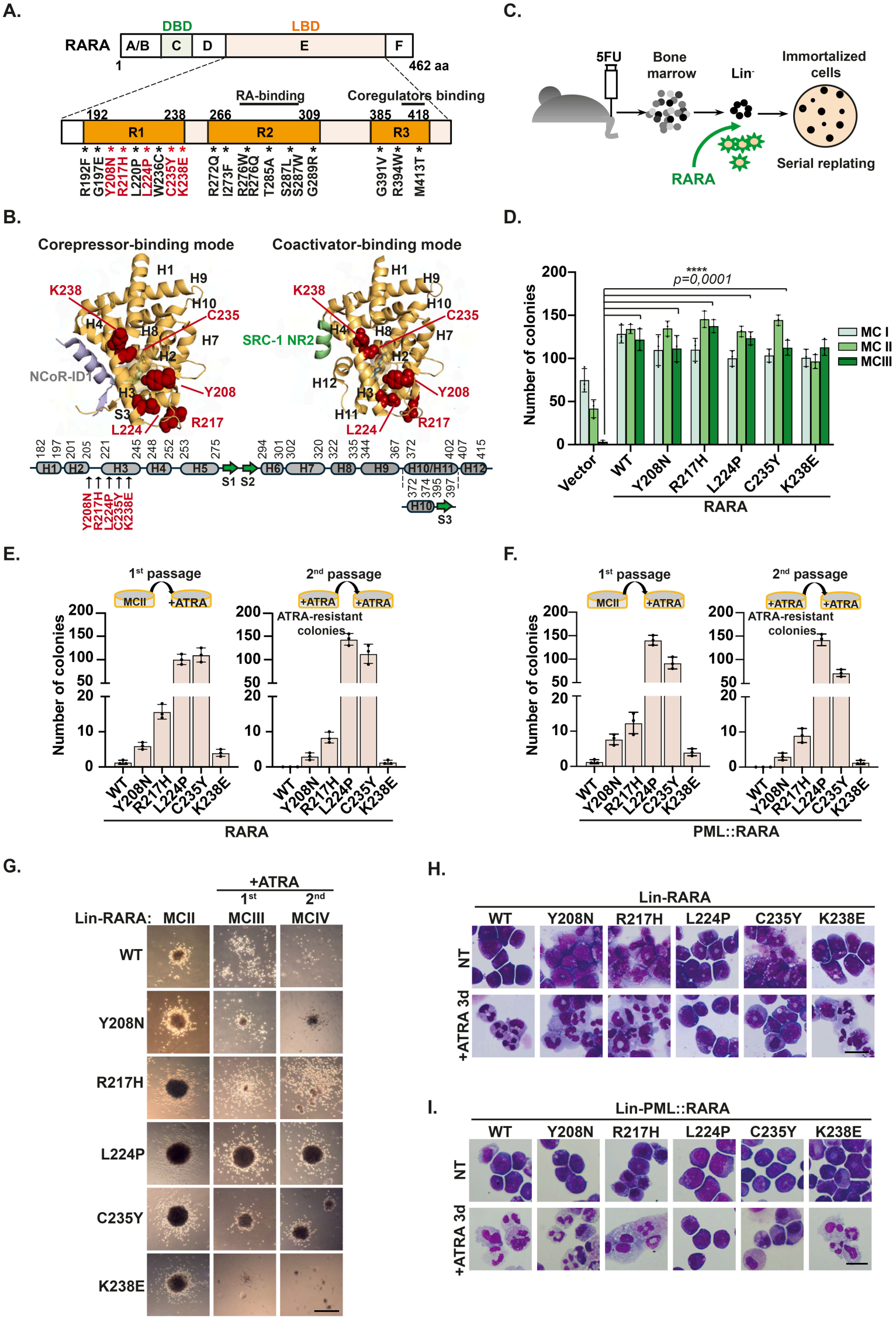
A.
DBD
LBD
RARA
A/B
C
D
E
F
1
462 aa
RA-binding
Coregulators binding
192
238
266
309
385
418
R1
R2
R3
R192F * * G197E Y208N * R217H * L220P L224P * W236C * C235Y * * K238E
R272Q * * I273F R276W * R276Q T285A * S287L * S287W G289R *
G391V * R394W * M413T *
B.
Corepressor-binding mode
Coactivator-binding mode
K238
H1
H9
H10
C235
H4
H8
H7
H2
NCoR-ID1
H3
Y208
S3
L224
R217
SRC-1 NR2
H12
H11
182 197 201 205 221 245 248 252 253 275 294 301 302 320 322 335 344 367 372 402 407 415
H1 H2 H3 H4 H5 S1 S2 H6 H7 H8 H9 H10/H11 H12
372 374 395 397
H10 S3
Y208N R217H L224P C235Y K238E
C.
5FU
Bone marrow
Lin-
Immortalized cells
RARA
Serial replating
D.
Number of colonies
200
150
100
50
0
****
p=0,0001
MC I
MC II
MCIII
Vector
WT
Y208N
R217H
L224P
C235Y
K238E
RARA
E.
1st passage
2nd passage
MCII
+ATRA
ATRA-resistant colonies
Number of colonies
200
150
100
50
20
10
0
WT
Y208N
R217H
L224P
C235Y
K238E
RARA
F.
1st passage
2nd passage
MCII
+ATRA
ATRA-resistant colonies
Number of colonies
PML::RARA
G.
+ATRA
1st
2nd
Lin-RARA:
MCII
MCIII
MCIV
WT
Y208N
R217H
L224P
C235Y
K238E
H.
Lin-RARA
WT
Y208N
R217H
L224P
C235Y
K238E
NT
+ATRA 3d
I.
Lin-PML::RARA
WT
Y208N
R217H
L224P
C235Y
K238E
NT
+ATRA 3d

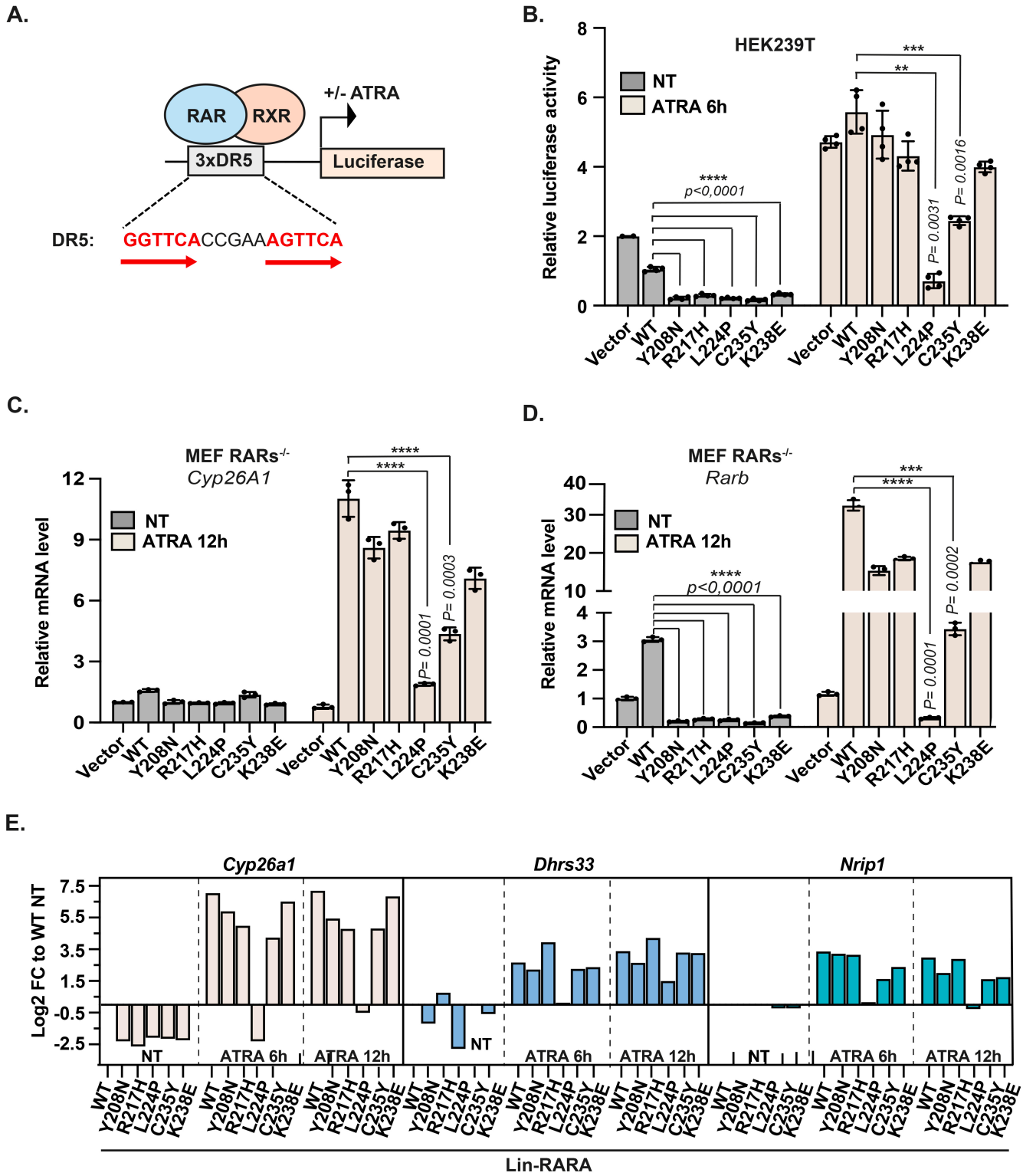
A.
RAR
RXR
+/- ATRA
3xDR5
Luciferase
DR5: GGTTCACCGAAAGTTCA
B.
HEK239T
NT
ATRA 6h
Relative luciferase activity
****
p<0,0001
***
**
P= 0.0031
P= 0.0016
Vector
WT
Y208N
R217H
L224P
C235Y
K238E
C.
MEF RARs-/-
Cyp26A1
NT
ATRA 12h
Relative mRNA level
****
****
P= 0.0001
P= 0.0003
D.
MEF RARs-/-
Rarb
NT
ATRA 12h
Relative mRNA level
***
****
****
p<0,0001
P= 0.0001
P= 0.0002
E.
Cyp26a1
Dhrs33
Nrip1
Log2 FC to WT NT
NT
ATRA 6h
ATRA 12h
Lin-RARA

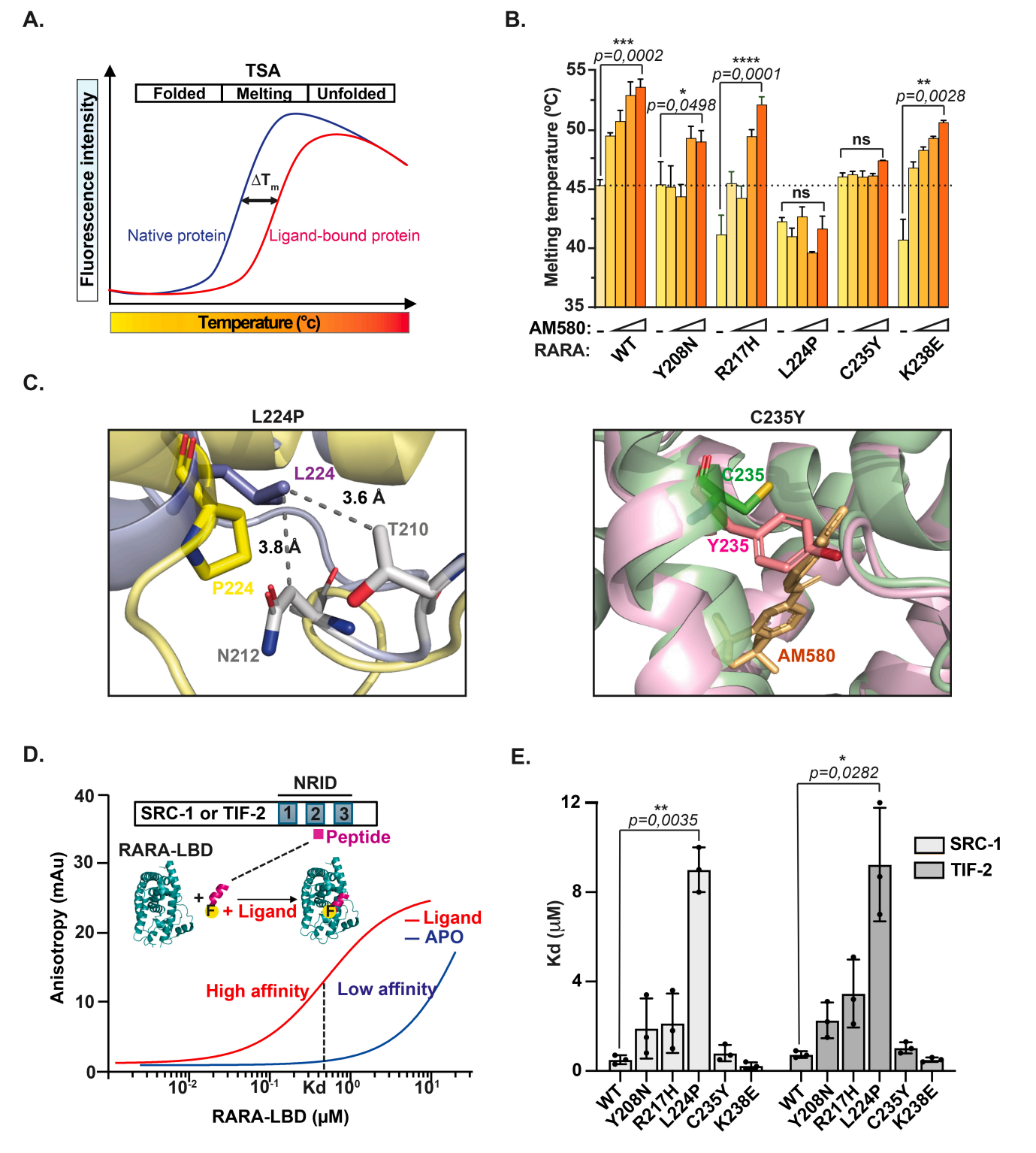
A.
TSA
Folded
Melting
Unfolded
Fluorescence intensity
ΔTm
Native protein
Ligand-bound protein
Temperature (°c)
B.
Melting temperature (°C)
***
p=0,0002
*
p=0,0498
****
p=0,0001
ns
ns
**
p=0,0028
AM580:
RARA:
WT
Y208N
R217H
L224P
C235Y
K238E
C.
L224P
L224
3.6 Å
T210
3.8 Å
P224
N212
C235Y
C235
Y235
AM580
D.
NRID
SRC-1 or TIF-2
1
2
3
Peptide
RARA-LBD
F
+ Ligand
Ligand
APO
High affinity
Low affinity
Anisotropy (mAu)
Kd
RARA-LBD (μM)
E.
**
p=0,0035
*
p=0,0282
SRC-1
TIF-2
Kd (μM)
WT
Y208N
R217H
L224P
C235Y
K238E

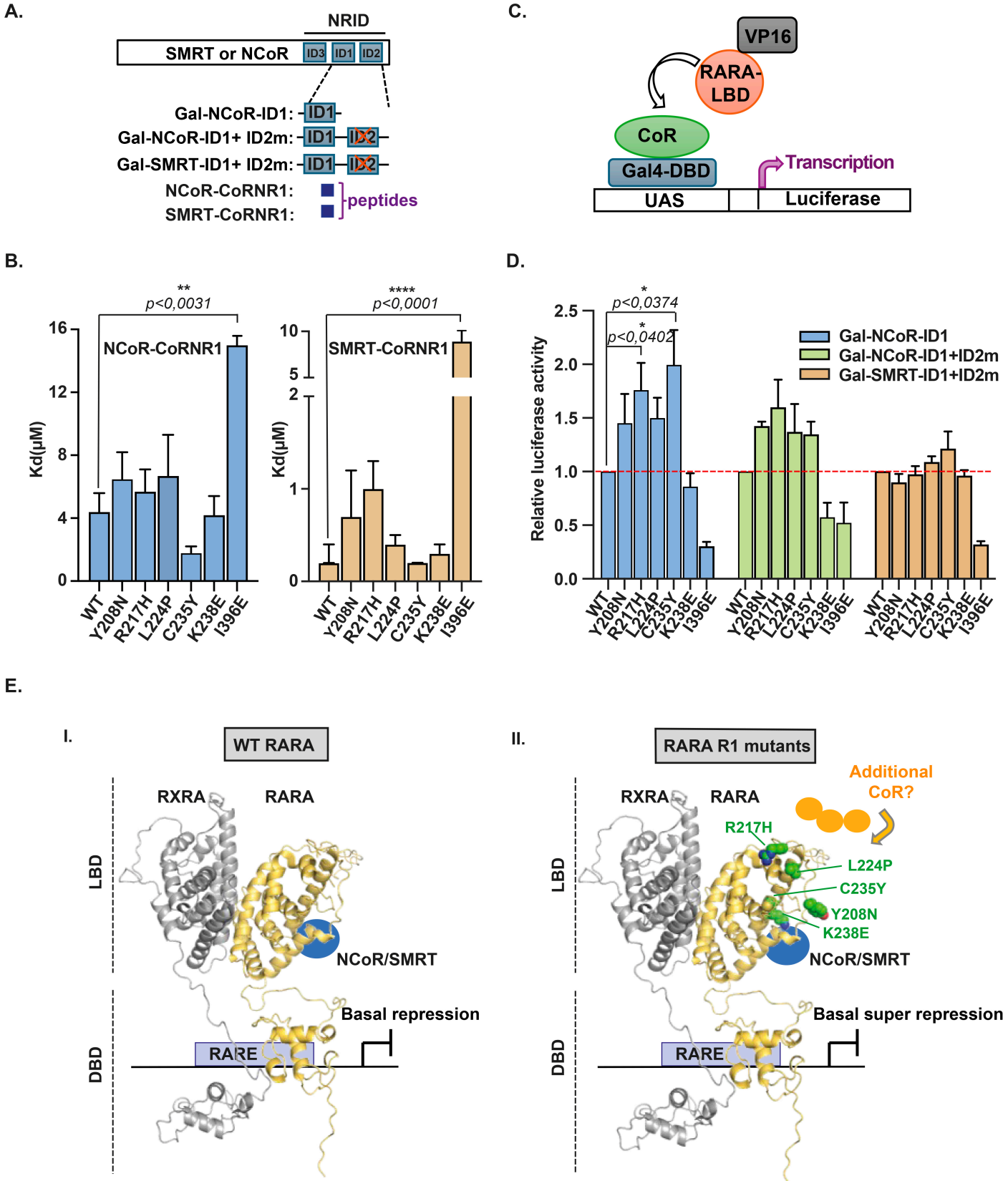
A.
NRID
SMRT or NCoR
ID3
ID1
ID2
Gal-NCoR-ID1:
Gal-NCoR-ID1+ ID2m:
Gal-SMRT-ID1+ ID2m:
NCoR-CoRNR1:
SMRT-CoRNR1:
peptides
C.
VP16
RARA-LBD
CoR
Gal4-DBD
Transcription
UAS
Luciferase
B.
**
p<0,0031
NCoR-CoRNR1
Kd(μM)
****
p<0,0001
SMRT-CoRNR1
WT
Y208N
R217H
L224P
C235Y
K238E
I396E
D.
*
p<0,0374
*
p<0,0402
Relative luciferase activity
Gal-NCoR-ID1
Gal-NCoR-ID1+ID2m
Gal-SMRT-ID1+ID2m
E.
I.
WT RARA
RXRA
RARA
LBD
DBD
NCoR/SMRT
Basal repression
RARE
II.
RARA R1 mutants
Additional CoR?
R217H
L224P
C235Y
Y208N
K238E
Basal super repression

SUPPLEMENTARY METHODS

Plasmid constructs and site-directed mutagenesis

The pSG5 and pMSCV-neomycin plasmids expressing human RARA or PML::RARA[1] were used for the luciferase and clonogenic assays, respectively. The pET15b-RARA (176-421) plasmid[2] was used for expression and purification of recombinant RARA LBD protein. The VP16-RARA (176-421) plasmid[2] was used for mammalian two-hybrid assay. RARA LBD mutants were generated from these plasmids using site-directed mutagenesis kit (Agilent Technologies) with primers listed in Table S2.

Ligands

Retinoic acid (#0695), AM580 (#0760) and BMS493 (#3509) ligands were purchased from Tocris Bioscience.

Cell culture

All cell lines commercially purchased or kindly gifted are listed here: HEK293T (ATCC, #CRL-3216), COS-7 (ATCC, #CRL-1651), Plat-E (Cell biolab Inc, #CB-RV-101) and immortalized MEF RARs$^{-/-}$ in which *RARA, RARB, RARG* genes were functionally inactivated by the CRE-Lox technology (Henrich Gronemeyer, IGBMC, Strasbourg, France)[3]. Cell lines were grown in DMEM GlutaMAX medium with 10% fetal calf serum supplemented with 100 U/ml of penicillin/streptomycin and maintained at 37°C with 5% CO_2. When required blasticidin-S (10ug/ml) and puromycin (1ug/ml) were added to the culture medium of the retroviral packaging cell line (Plat-E) to ensure the stable expression of the viral structural proteins[4]. Cells were transfected with the indicated plasmids using polyethyleneimine (Sigma-Aldrich) or JetPei transfectant agent (Ozyme) according to the manufacturer's recommendation.

Colony-forming cell assay

Bone marrow cells were harvested from C57BL/6 mice at five days post-injection of 5-

fluorouracil (5-FU) (150 mg/kg) to recover lineage-negative (Lin^-) cells using a lineage depletion kit (Miltenyl Biotec). Lin^- cells were then retrovirally transduced with RARA mutants in the presence of polybrene (8ug/ml, Sigma-Aldrich) and grown in a methylcellulose-base medium (M3234, Stemcell Technologies) supplemented with murine cytokines (mIL3 (10ng/ml), mIL6 (10ng/ml), mGM-CSF (10ng/ml), mSCF (50ng/ml), Stemcell Technologies) and G418 (1ug/ml, Sigma-Aldrich) to select RARA-immortalized blasts. Serial replating of G418-resistant colonies at a density of 10,000 cells per well in 6-well plates was performed up to four passages and colonies number was scored at each passage. For microarray analysis, immortalized-Lin^- progenitors were recovered at passage III and grown in StemSpan SFEM liquid medium (Stemcell Technologies) supplemented with the same cytokine cocktail described above. When required, cells were exposed to 1 µM of ATRA for 6h or 12h.

May-Grünwald Giemsa staining

To monitor RA-induced changes in immortalized blasts, 1x 10^5 cells were cyto-spined onto glass microscope slides at 400x *g* for 5 min. May-Grünwald Giemsa staining was performed on an automated stainer for human medical cell diagnosis in Saint-Louis hospital and cell morphology were observed under a bright-field light microscope.

Western blot analysis

HEK293T cells were transfected with pSG5-RARA or PML::RARA constructs and exposed to 1 µM ATRA the following day. Cells were harvested 48h post-transfection, washed once with 1X PBS, and lysed in 2X Laemmli buffer (Sigma-Aldrich). After clarification by ultrasonication (Diagenode), total cell extracts were resolved by SDS-PAGE and transferred onto a nitrocellulose membrane (Bio-Rad) for immunodetection using specific antibodies (rabbit anti-RARA (homemade, S.Kogan, USA), mouse anti-ßactin (A3854, Sigma-Aldrich), and goat anti-rabbit IgG-HRP (111-035-045, Jackson immune research)). Proteins were detected using the Dura ECL chemiluminescence reagents (ThermoFisher) and the Vilber Fusion-Fx (BIO-1D v15-07) imaging system. Band intensities for RARA and actin loading control were measured

using Image J software to compare protein level in RARA LBD mutants.

Real-time quantitative polymerase chain reaction

Total RNA was extracted from immortalized blasts or transduced MEF cells using the RNeasy Plus Mini kit (Qiagen) according to the manufacturer's protocol. cDNA was synthesized from 1 µg total RNA using the Maxima First Strand cDNA Synthesis kit (Thermo Fisher Scientific) with random hexamer primers and oligo(dT). Quantitative real-time PCR was performed on a Roche LightCycler 480 using FastStart SYBR Green Master Mix (Roche) and gene expression levels were normalized to *Gapdh* housekeeping gene using the ΔΔCt method. Gene-specific primers are listed in Table S2.

Microarray transcriptomic data analysis

Total RNA samples were prepared from immortalized-RARA blasts at passage III before and after ATRA treatment (6 h and 12 h) for whole-transcriptome genome analysis using the GeneChip Plus Reagent Kit (ThermoFisher Scientific). Each sample was hybridized to a GeneChip® Mouse transcriptome array 1.0 (ThermoFisher Scientific) with the Affymetrix® Fluidics Station 450. Arrays were scanned with the Affymetrix GeneChip Scanner 3000 7G, and raw CEL files were processed using Affymetrix Transcriptome Analysis Console (TAC) software (v4.0) with default settings (RMA normalization, background correction). Differential gene expression (fold-change > 2.0, FDR < 0.05) of *Rara* mutant versus *Rara*^{wt} was compared at basal condition and also after 6 h or 12 h ATRA treatment.

Expression and purification of recombinant RARA LBD proteins

The WT and RARA LBD mutants were expressed from the pET15b-RARA (176-421) vector and purified by standard affinity chromatography as previously described[2]. Quality control of purified proteins was achieved by SDS-PAGE while their structural integrity was validated by circular dichroism and dynamic light scattering as described below.

Circular dichroism

The protein secondary structures were determined by far UV-circular dichroism spectroscopy using a Chirascan instrument (Applied Photophysics). Protein samples (1 mg/ml in 20 mM Tris pH 7.5, 150 mM NaCl) were loaded in quartz cuvettes, 0.1 mm path length (Hellma), and the wavelength scans were obtained between 190 and 260 nm, step size 0.5 nm, bandwidth 1 nm. Three different measurements were done for each sample. The mean value of the three measurements was buffer corrected and converted to mean molar residue ellipticity [θ] (deg×cm2/dmol).

Dynamics Light Scattering

The diameter size of RARA LBD protein samples (1 mg/ml in 20 mM Tris pH 7.5, 150 mM NaCl) were evaluated using the NanoStarPro (Wyatt).

Mammalian two-hybrid assays

The assay was performed as previously described[2]. Briefly, plasmids containing Gal-DBD coupled to corepressors (SMRT-ID1, NCoR-ID1[5], SMRT-ID1+ID2m, NCoR-ID1+ID2m[5]), VP16 linked to RARA LBD, and the $(17m)_{5x}$-G-Luc reporter gene were co-transfected into COS-7 cells. Luciferase activity was determined 48h post-transfection by using a luciferase assay kit (Promega). Results were normalized by the total protein concentration. Each transfection was executed in duplicate and repeated independently three times.

Thermal Shift Assay (TSA)

Thermal stability of RARA LBD mutants was assessed using a qPCR Mx3005P machine (Agilent Technologies) to follow the fluorescence emission of the SYPRO Orange dye during a temperature ramp from 25 to 95 °C (1°C increment). Protein and dye were mixed in a buffer containing 20 mM Tris HCl pH 7.5, 150 mM NaCl, 2 mM DTT at a final concentration ranging from 1 to 5 µM and 1x or 2x, respectively. Ligand (AM580 or BMS493) were added at 0.25–2-fold molar excess. Fluorescence was recorded (excitation 545 nm, emission 568 nm), and

melting temperatures (T_m) were determined by fitting triplicate data to a Boltzmann model using TSA Craft[6].

Steady-state fluorescence anisotropy

Binding assays were performed as previously described[2], using a Safire microplate reader (TECAN). The fluorescent peptides listed in Table S3 were purchased from EZBiolab. Excitation/emission wavelengths were 470/530 nm for fluorescein- and 530/580 nm for tetramethylrhodamine-labeled peptides. The buffer solution was 20 mM Tris-HCl, pH 7.5, 150 mM NaCl, 2 mM DTT and 10% (v/v) glycerol. Protein (10 or 20 µM) was serially diluted and mixed with 4 nM fluorescent peptide ± ligand (20 or 40 µM). Dissociation constants (Kd) were determined by nonlinear regression with a sigmoidal dose-response model (GraphPad Prism, GraphPad Software). The reported data are the average of at least three independent experiments.

Molecular Dynamics Simulation

RARA Structure Modeling - The RARA LBD was modeled in its repressive conformation using Alphafold 3.0[7]. To keep its repressive state, we modeled the receptor in the presence of the corepressor, which was removed later on. The sequence was the same as the one used in the experiments. The model presented high similarity (RMSD: 0.369 Å) to the crystallographic structure of RARA bound to the CoRNR1 of NCoR and the inverse agonist ligand BMS493 (PDB: 3KMZ)[2]. H12 was reconstructed as a random coil (extracted from[8]). For the L224P RARA model preparation, the leucine at position 224 was replaced with a proline in the same model using the PyMOL Molecular Graphics System. The SCWRL4 program was further used to refine and validate the side chain predictions, specifically regarding the new mutated residue[9].

MD simulations setup - The CHARMM-GUI web interface[10] was used to prepare the MD simulations of the WT and L224P RARA LBDs. The PROPKA server for pKa prediction was

also used to determine the protonation states of histidines[11]. The CHARMM36 all atom force field was used[12, 13] and the simulations were performed with the NAMD program[14, 15]. The protein was solvated in a cubic water box with dimensions of 110 Å in the X, Y, and Z directions, and sodium and chloride ions were added to achieve a neutral system with a final ion concentration of 0.15 M. The system was equilibrated at 303.15 K following energy minimization for 10,000 steps. During the equilibration, a 2-femtosecond (fs) integration time step was used, and bonds involving hydrogen atoms were constrained using the rigidBonds algorithm. Langevin dynamics was employed for temperature control with a damping coefficient of 1 ps^{-1}. The electrostatics were treated using the Particle Mesh Ewald (PME) method with a grid spacing of 1.0 Å and an interpolation order of 6. Nonbonded interactions were smoothly switched off between 10 and 12 Å, and a pair list cutoff of 16 Å was applied. Periodic boundary conditions were used, and atomic positions were wrapped to the primary unit cell. During this phase, positional restraints were applied to the protein atoms using a reference structure and the system was equilibrated for 250 ps. The positional restraints were removed and the production simulation was initiated from the equilibrated system at 303.15 K and was calculated for 100 nanoseconds (ns), with six replicates performed for each protein variant. Nonbonded interactions were handled with a cutoff of 12 Å and a switching function that began at 10 Å. The temperature was maintained using Langevin dynamics, and frames were saved every 500 fs (250 steps).

Data analysis – Root-mean-square fluctuations (RMSF) were computed and averaged from all the trajectories using MDAnalysis[16, 17]. To evaluate the minimal inter-residue contacts involving residue 224 under mutant and WT conditions, we computed the contacts frame by frame using by MDAnalysis. Distance distributions were plotted as normalized histograms using 30 bins from 0 to 10 Å and expressed as probability densities. A cutoff of 4.5 Å was used to identify potential residue-residue contacts. The resulting distributions were visualized as overlaid curves plotted using GraphPad Prism.

Pocket Calculations

The DoGSite3 program [18] was used to predict and measure the binding pocket volumes of RARA in its wild-type and C235Y mutant forms.

Docking calculations

The AutoDock program version 4.2 was used to dock ATRA and AM580 to their respective crystallographic structures in both wild-type, PDBIDs[19] and 3KMR[2], respectively, and their C235Y mutant forms; the latter were constructed using the crystal structure followed by the introduction of the mutation using the SCRWL4 program[9]. The calculations were piloted using AutoDockTools (20) (ADT). The ligands were taken from the crystal structures and protonated using the Avogardo software[21]. The partial charges of the atoms were taken to be the default values assigned by the AutoDock program. AutoGrid4 was used to pre-calculate the grid maps corresponding to interaction energies of the different atom types present in the systems. The grid was placed over the region including the ligand binding pocket, H12 and the omega loop. The Lamarckian Genetic Algorithm (LGA) was used to get favorable conformations, which were then clustered according to a Root Mean Square Deviation (RMSD) threshold of 2.0 Å per docked molecule. The ranking of clusters was based on the best-estimated binding free energy in kcal/mol for each cluster. We retained the conformations for further analysis.

SUPPLEMENTARY TABLES

Table S1. List of RARA LBD mutations described in the literature and causing APL.

Mutations	Reference
R192C	22
E197G	23
K207N	22
Y208N	24
R217H/S	24, 25
V218D	26
L220P	27
L224I/P	23, 24
W225C/R	22
C235F	27
K238E	24
R272Q/G	22, 24, 26-29
I273F	24
R276Q/T/W	22, 24, 27, 29
T278A	26
T283I	23
M284V	23
T285A/I	24, 27, 28
S287W/L	23, 24, 27
D288E	23
G289E/R	23, 30
L290V	27, 30
T291A/I	26, 27
R294W	26, 30
H298N	22
N299D	26
A300G	26
G391V	22
R394W	31
E421D	22
M413T	30, 31
Insertion/deletions	
K207-Y208del	24
L220_F228delinsP	26
K227-T233 del	25
R394-L398/394Mdel	30
E412-L414del	24

Table S2. List of primers used in the study.

RARA mutants	Primers for mutagenesis
Y208N	For: 5'-gttgttcgtagtgtttttgcccagctggcagag-3' Rev: 5'-ctctgccagctgggcaaaaacactacgaacaac-3'
R217H	For: 5'-caatgtccagagagacatgttgttctgagctgttg-3' Rev: 5'-caacagctcagaacaacatgtctctctggacattg-3'
L224P	For: 5'-cactgaacttgtcccaggggtcaatgtccagagag-3' Rev: 5'-ctctctggacattgacccctgggacaagttcagtg-3'
C235Y	For: 5'-gaactccacagtcttaatgatatacttggtggagagttcactga-3' Rev: 5'-tcagtgaactctccaccaagtatatcattaagactgtggagttc-3'
K238E	For: 5'-actccacagtctcaatgatgcacttggtggagagtt-3' Rev: 5'-aactctccaccaagtgcatcattgagactgtggagt-3'
	Primers for RT-qPCR
mCyp26A1	For: 5'-ccggcttcaggctacaga-3' Rev: 5'-ggagctctgttgacgattgtt-3'
mRarb	For: 5'-agcccaccaggaaacctt-3' Rev: 5'-cagaggcccaagtccaatc-3'
mGapdh	For: 5'-gggttcctataaatacggactgc-3' Rev: 5'-ccattttgtctacgggacga-3'

Table S3. Sequence of the coregulator peptides used for steady-state fluorescence anisotropy assays.

Peptide	Sequence	Fluorescent probe
SMRT CoRNR1	RVVTLAQHISEVITQDYTR	Tetramethylrhodamine
NCoR CoRNR1	RLITLADHICQIITQDFAR	Fluorescein
TIF-2 NR2	KHKILHRLLQDSS	Fluorescein
SRC-1 NR2	RHKILHRLLQEGS	Fluorescein

SUPPLEMENTARY FIGURES

Figure S1: Analysis of RARA LBD mutations in ATRA-resistant APLs and BFT. (A) RARA LBD mutational landscape reported in APL and breast cancer tumors (BFT) based on clinical studies reported in Table 1. **(B)** Overall distribution of RARA LBD mutations in both APL and BFT.

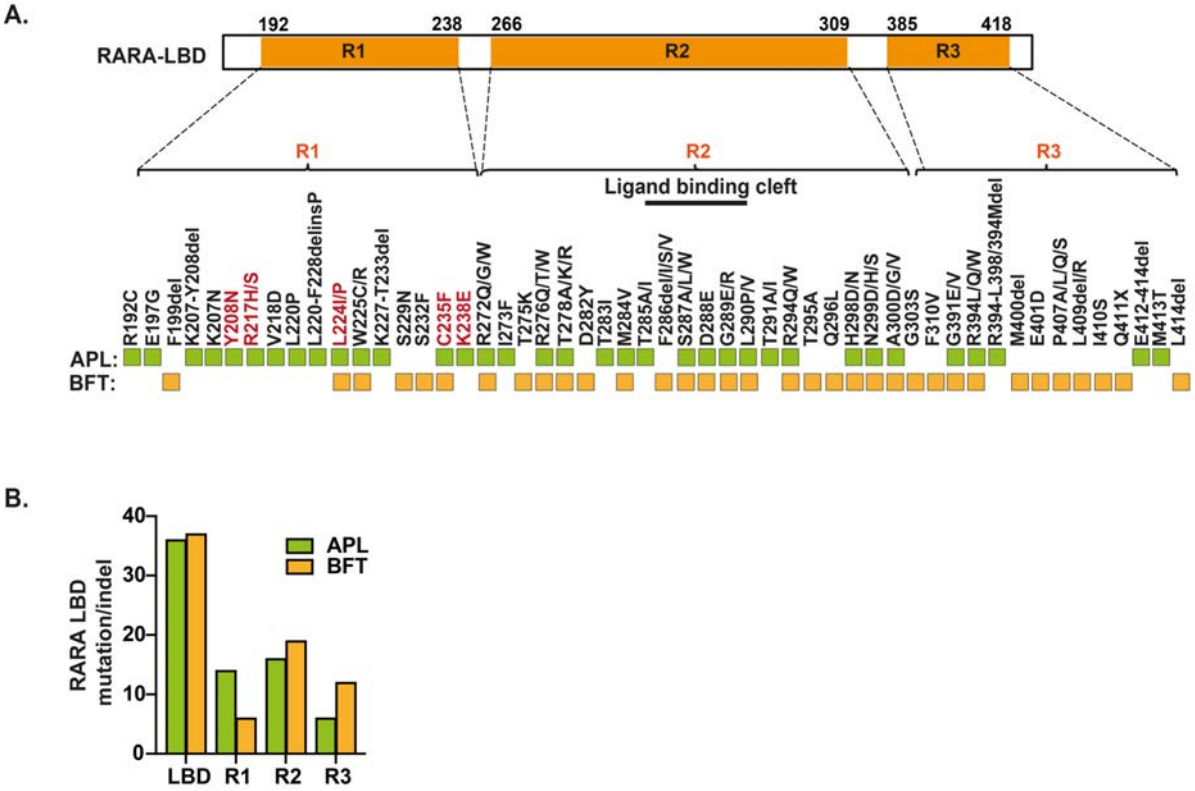

Figure S2: Clonogenic activity and ATRA-induced degradation of PML::RARA R1 mutants. (A) Schematic representation of PML::RARA gene showing five missense mutations identified in RA-resistant APL patients and located in the R1 domain of RARA LBD. DBD: DNA binding domain; LBD: Ligand binding domain. **(B)** Western blot analysis showing PML::RARA expression in immortalized Lin progenitors at passage III. **(C)** Serial replating assay showing colony counts from 10^4 cells grown in methylcellulose for three passages (MCI to MCIII). Graph shows means +/- SD of n=3 biological replicates by two-tailed unpaired t test with Welch's correction comparing PML:: RARA R1 mutants to vector at passage III (**** p<0,0001). **(D)** PML::RARA colony images before and after 2nd passage with ATRA. Scale bar= 200 µm. **(E-F)** Western blot analysis of PML::RARA and RARA R1 mutants transfected in HEK293T cells and exposed or not to 10 µM ATRA for 24 h. Data are representative of three independent experiments.

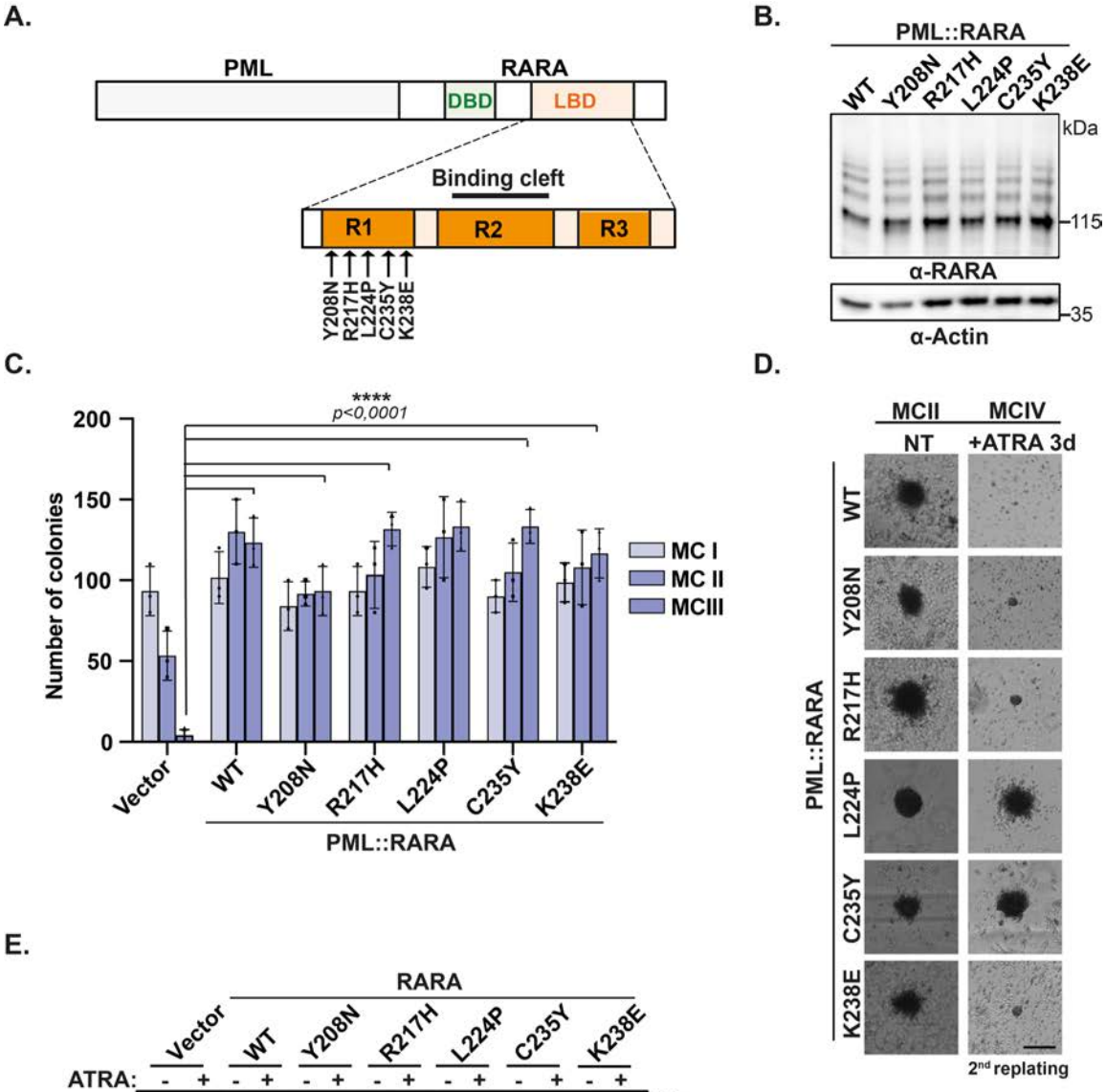
A.
PML
RARA
DBD
LBD
Binding cleft
R1
R2
R3
Y208N
R217H
L224P
C235Y
K238E
B.
PML::RARA
WT
Y208N
R217H
L224P
C235Y
K238E
kDa
115
α-RARA
35
α-Actin
C.
****
p<0,0001
Number of colonies
200
150
100
50
0
MC I
MC II
MCIII
Vector
WT
Y208N
R217H
L224P
C235Y
K238E
PML::RARA
D.
MCII
MCIV
NT
+ATRA 3d
PML::RARA
WT
Y208N
R217H
L224P
C235Y
K238E
2nd replating
E.
RARA
Vector
WT
Y208N
R217H
L224P
C235Y
K238E
ATRA:
- + - + - + - + - + - + - +
kDa
α-RARA
50
α-Actin
40
F.
PML::RARA
Vector
WT
Y208N
R217H
L224P
C235Y
K238E
ATRA:
- + - + - + - + - + - + - +
kDa
α-RARA
115
α-Actin
40

Figure S3: Transcriptional activity of PML::RARA R1 mutants. **(A)** Graph showing transcriptional activities of PML::RARA R1 mutants in the presence of 100 nM ATRA or AM580 for 12h. Relative luciferase activity corresponds to the ratio of firefly to renilla luciferase signal (means +/- SD of n = 3). **(B)** Western blot analysis of MEF RARs$^{-/-}$ transduced with WT and PML::RARA R1 mutants. **(C)** Rt-qPCR analysis of *CYP26B1* in MEF RAR$^{-/-}$ cells transduced with PML::RARA R1 mutants and exposed to vehicle or 100 nM ATRA for 12h. Graph shows means +/- SD of n=3 biological replicates by two-tailed unpaired t test with Welch's correction comparing L224P and C235Y mutants to WT(**p<0,01).

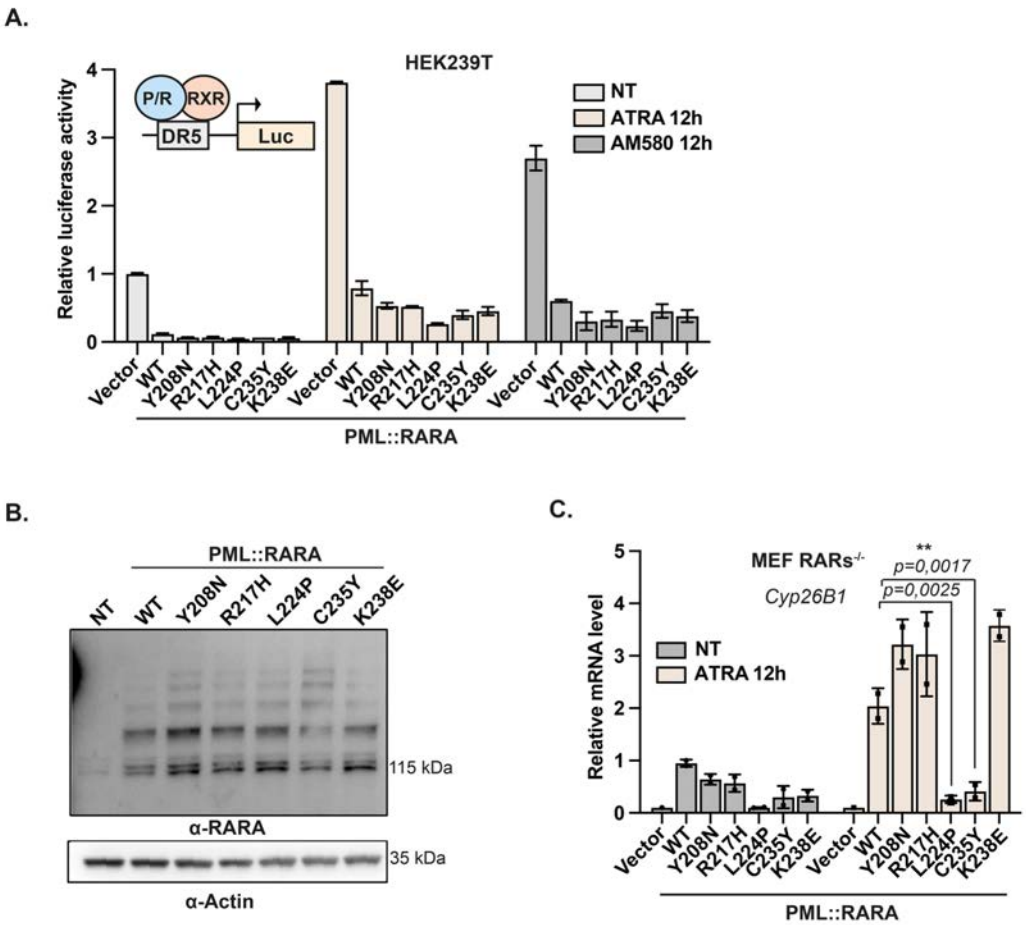

Figure S4: Characterization of mutant RARA LBDs. (A) Coomassie-stained SDS-page of the purified WT and RARA LBDs mutants. **(B)** Melting temperature of WT and RARA R1 mutants measured by TSA in the presence of increasing BMS493 concentrations. Columns from left to right represent protein-ligand ratios: 1:0; 1:0.25; 1:0.5; 1:1; and 1:2. Graph shows means +/- SD of n=3 independent biological replicates. **(C)** Molar ellipticity, in deg.cm^2/dmol, of WT and mutant RARA LBDs assessed by far-UV circular dichroism (CD). **(D)** Diameter size, in nm, of the globular WT and RARA LBDs mutants determined by dynamic light scattering (DLS) All the proteins have a high helical content corresponding to a folded LBD and a hydrodynamic diameter around 7 nm corresponding to a monomeric form of the LBD in solution. **(E)** Atomic fluctuations in WT and L224P RARA LBDs as determined by the calculation of root mean square fluctuation (rmsf) during molecular dynamics simulations. The color scale and the thickness of the 3D structure reflect the flexibility: thin and blue regions are less flexible and thick and red regions are more flexible. **(F-H)** Graphs of probability density versus distance reflecting the overall distribution of distances over molecular dynamics simulations around the residue L224 (WT in brown) and P224 (mutant in blue) regarding the interacting residues T210 (F), N212 (G) (both in H2-H3 loop) and F286 (H) (in the LBP). This information reflects the probability of the contacts between two analyzed residues, as illustrated in the zoom of the region around residues L224 in the WT and P224 in the mutant. Arrows indicate variations in distances between residues of interest in the two first panels, and the double arrow indicate the formation of a CH/π interaction in the last panel.

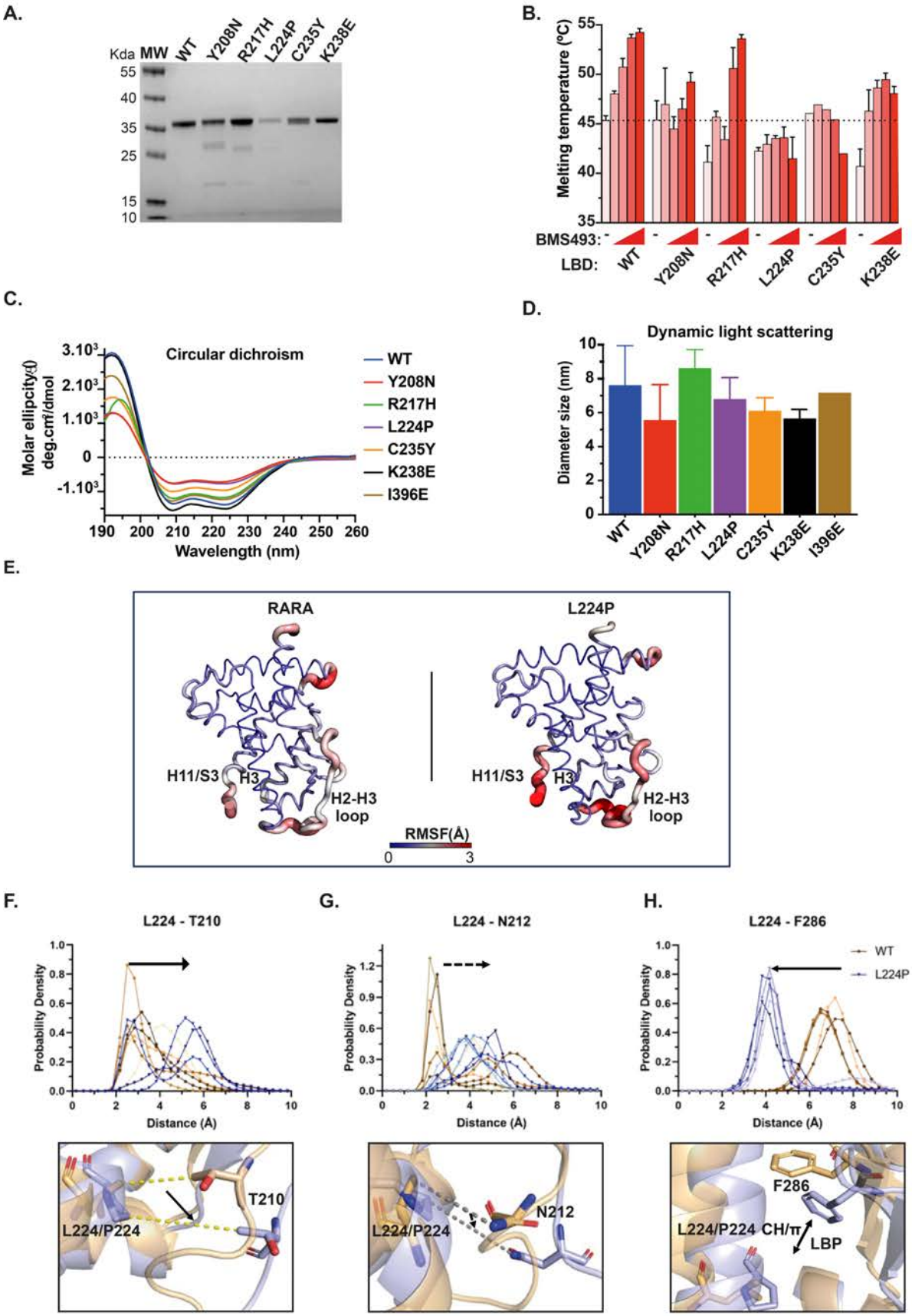
A.
Kda MW WT Y208N R217H L224P C235Y K238E
55
40
35
25
15
10
B.
Melting temperature (°C)
55
50
45
40
35
BMS493: - - - - - -
LBD: WT Y208N R217H L224P C235Y K238E
C.
Circular dichroism
Molar ellipcity deg.cm²/dmol
3.10³
2.10³
1.10³
0
-1.10³
190 200 210 220 230 240 250 260
Wavelength (nm)
WT
Y208N
R217H
L224P
C235Y
K238E
I396E
D.
Dynamic light scattering
Diameter size (nm)
10
8
6
4
2
0
WT Y208N R217H L224P C235Y K238E I396E
E.
RARA
L224P
H11/S3
H3
H2-H3 loop
RMSF(Å)
0 3
F.
L224 - T210
Probability Density
Distance (Å)
T210
L224/P224
G.
L224 - N212
Probability Density
Distance (Å)
N212
L224/P224
H.
L224 - F286
WT
L224P
Probability Density
Distance (Å)
F286
L224/P224 CH/π
LBP

Figure S5: Functional dose-response analysis of retinoid in RARA R1 mutants.

Transcriptional activities of RARA R1 mutants measured by dual-luciferase reporter assay in HEK293T cells after 12h exposure to a range of ligand concentrations (ATRA or AM580; 10^{-10} M to 10^{-5} M). Graphs show dose-response curves representing relative luciferase activity as mean +/- SD of n = 3 biological replicates.

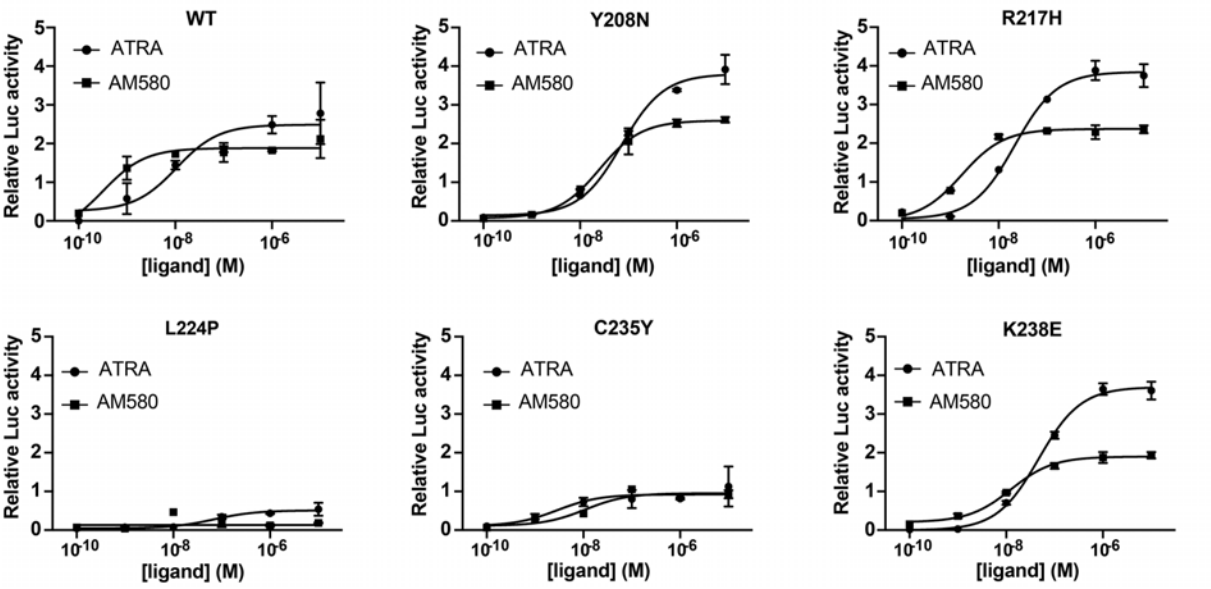

Figure S6: Structural analysis of ATRA and AM580 binding to the C235Y RARA mutant. **(A-B)** Results of ten AutoDock calculations on C235Y RARA mutant, in the presence of AM580 (A) or ATRA (B). The docked ligands AM580 and ATRA (shown as green or cyan sticks, respectively) are superposed on the RARA structure where the C235Y residue is shown as blue stick. **(C)** 2D interaction map of AM580 in the WT RARA LBP (PDB: 3KMR), highlighting canonical hydrogen bonds and hydrophobic contacts. 2D interaction maps from two representative flexible docking poses of AM580 in C235Y RARA LBP, showing altered ligand orientation, loss of hydrogen bound and changes in hydrophobic contacts. **(D)** 2D interaction map of ATRA in the WT RARA LBP (PDB: 3A93), highlighting hydrogen bonding with Ser287 and extensive hydrophobic contacts. Circled residues indicate interactions conserved between WT and RARA mutant complexes. 2D interaction maps from rigid and flexible docking poses of ATRA in C235Y RARA LBP. Rigid docking shows loss of the Ser287 hydrogen bond with reduction and reorganization of hydrophobic interactions whereas flexible docking shows altered ligand orientation and partial retention of hydrophobic contacts within the pocket.

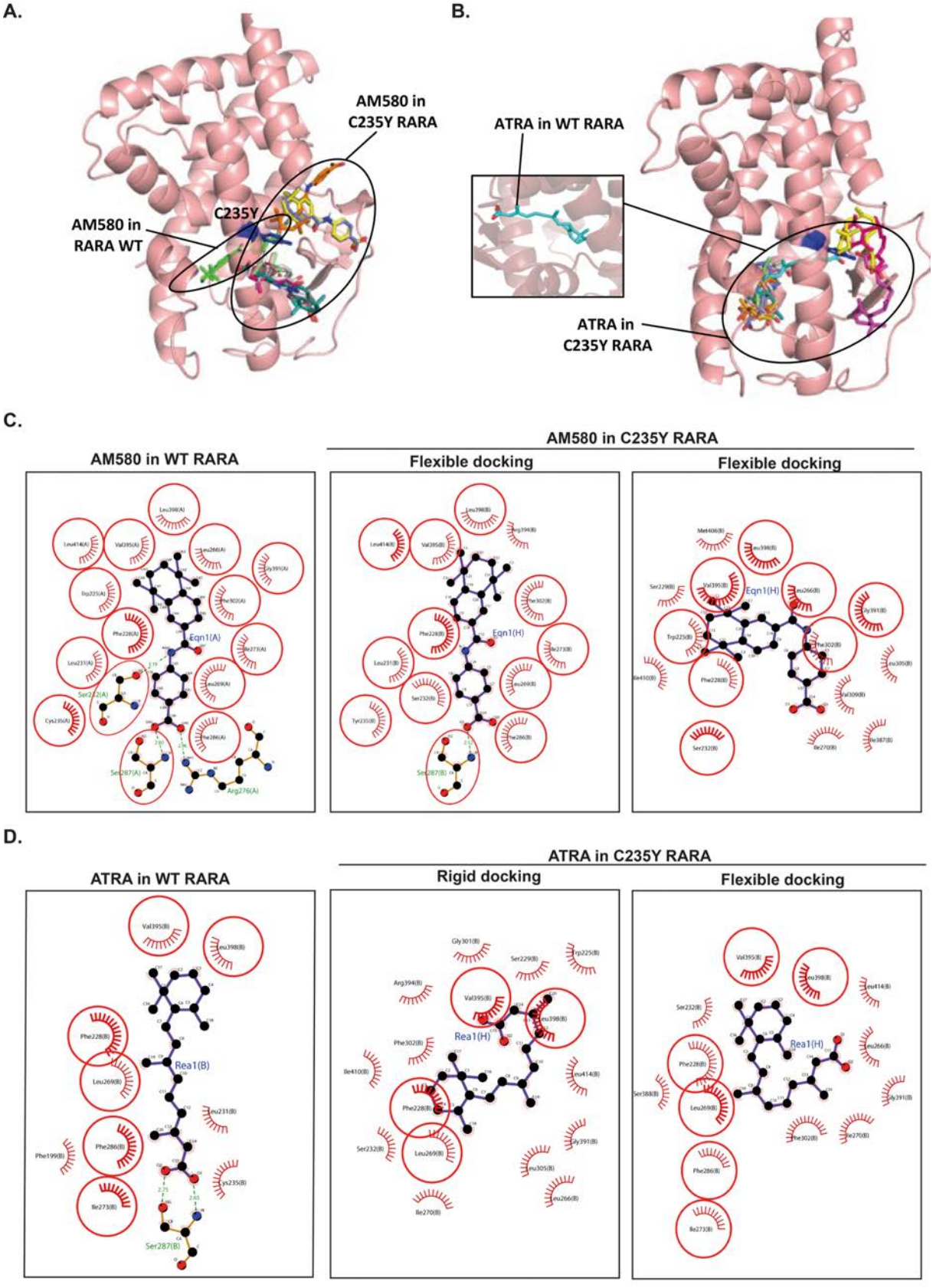
A.
AM580 in
C235Y RARA
C235Y
AM580 in
RARA WT
B.
ATRA in WT RARA
ATRA in
C235Y RARA
C.
AM580 in WT RARA
AM580 in C235Y RARA
Flexible docking
Flexible docking
D.
ATRA in WT RARA
ATRA in C235Y RARA
Rigid docking
Flexible docking

Figure S7: Titration curves of fluorescently-labelled coactivator peptides (SCR-1 and TIF-2 NR2) by WT and RARA LBD mutants, in the absence (**A-C**) and in the presence of RAR agonist AM580 (**B-D**). The results represent the average of at least three independent measurements. The bars are the SEM.

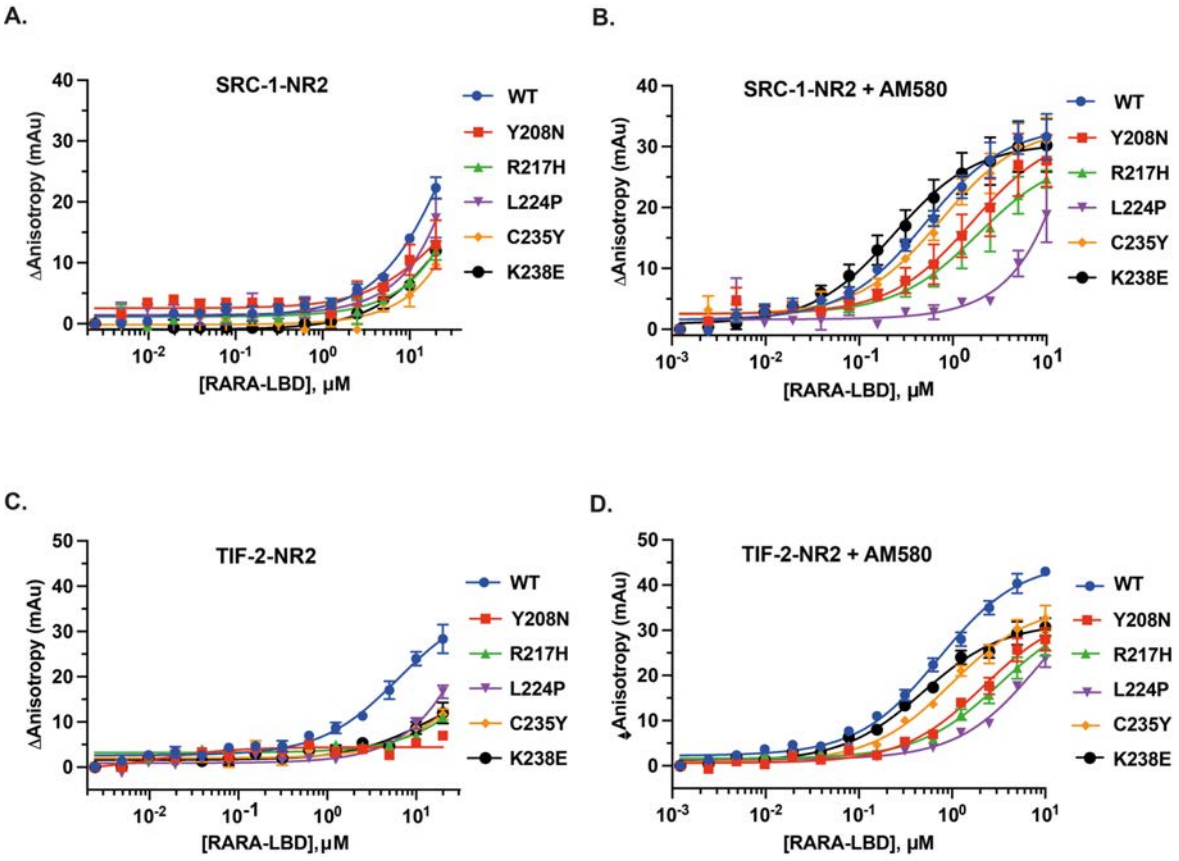

Figure S8: Titration curves of fluorescently-labelled corepressor peptides (NCoR and SMRT CoRNR1) by WT and m RARA LBD mutants, in the absence of ligand (**A-B**). The results represent the average of at least three independent measurements. The bars are the SEM.

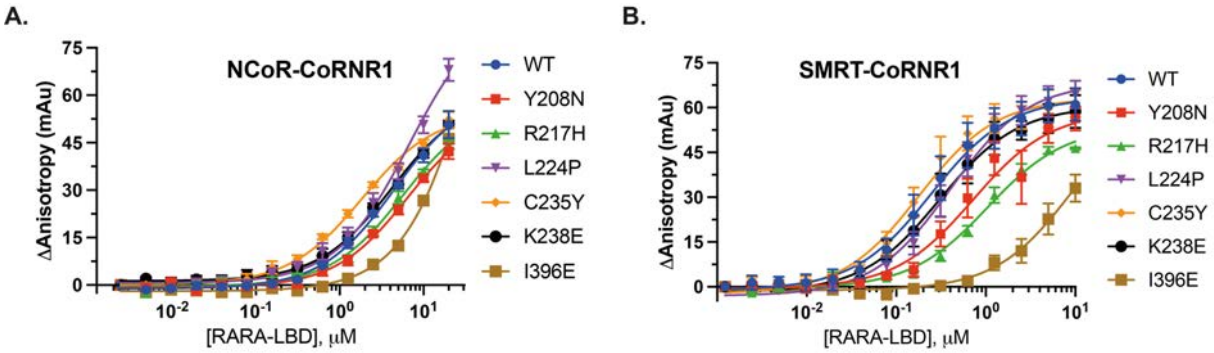

SUPPLEMENTARY REFERENCES

1. Zhu J, Gianni M, Kopf E, et al. Retinoic acid induces proteasome-dependent degradation of retinoic acid receptor alpha (RARalpha) and oncogenic RARalpha fusion proteins. Proc Natl Acad Sci U S A. 1999;96(26):14807-14812.

2. le Maire A, Teyssier C, Erb C, et al. A unique secondary-structure switch controls constitutive gene repression by retinoic acid receptor. Nat Struct Mol Biol. 2010;17(7):801-817.

3. Altucci L, Rossin A, Hirsch O, et al. Rexinoid-triggered differentiation and tumor-selective apoptosis of acute myeloid leukemia by protein kinase A-mediated desubordination of retinoid X receptor. Cancer Res. 2005;65(19):8754-8765.

4. Morita S, Kojima T, Kitamura T. Plat-E: an efficient and stable system for transient packaging of retroviruses. Gene Ther. 2000;7(12):1063-1066.

5. Hu X, Lazar MA. The CoRNR motif controls the recruitment of corepressors by nuclear hormone receptors. Nature. 1999;402(6757):93-96.

6. Reys V. Kowalewski J, Gelin M, et al. wTSA-CRAFT: an open-access web server for rapid analysis of thermal shift assay experiments. Bioinformatics Advances. 2023; 3(1):vbad136

7. Abramson J, Adler J, Dunger J, et al. Accurate structure prediction of biomolecular interactions with AlphaFold 3. Nature. 2024;630(8016):493-500.

8. Cordeiro TN, Sibille N, Germain P, et al. Interplay of Protein Disorder in Retinoic Acid Receptor Heterodimer and Its Corepressor Regulates Gene Expression. Structure. 2019;27(8):1270-1285 e6.

9. Krivov GG, Shapovalov MV, Dunbrack RL, Jr. Improved prediction of protein side-chain conformations with SCWRL4. Proteins. 2009;77(4):778-795.

10. Jo S, Kim T, Iyer VG et al. CHARMM-GUI: a web-based graphical user interface for CHARMM. J Comput Chem. 2008;29(11):1859-1865.

11. Li H, Robertson AD, Jensen JH. Very fast empirical prediction and rationalization of protein pKa values. Proteins. 2005;61(4):704-721.

12. Huang J, MacKerell AD, Jr. CHARMM36 all-atom additive protein force field: validation based on comparison to NMR data. J Comput Chem. 2013 Sep 30;34(25):2135-2145.

13. MacKerell AD, Bashford D, Bellott M, et al. All-atom empirical potential for molecular modeling and dynamics studies of proteins. J Phys Chem B. 1998;102(18):3586-3616.

14. Lee J, Cheng X, Swails JM, et al. CHARMM-GUI Input Generator for NAMD, GROMACS, AMBER, OpenMM, and CHARMM/OpenMM Simulations Using the CHARMM36 Additive Force Field. J Chem Theory Comput. 2016;12(1):405-4013.

15. Phillips JC, Hardy DJ, Maia JDC, et al. Scalable molecular dynamics on CPU and GPU architectures with NAMD. J Chem Phys. 2020;153(4):044130.

16. Gowers R, MLinke M, Barnoud J, et al. MDAnalysis: A Python Package for the Rapid Analysis of Molecular Dynamics Simulations. Scipy. 2016:98–105.

17. Michaud-Agrawal N, Denning EJ, Woolf TB, et al: a toolkit for the analysis of molecular dynamics simulations. J Comput Chem. 201132(10):2319-2327.

18. Graef J, Ehrt C, Rarey M. Binding Site Detection Remastered: Enabling Fast, Robust, and Reliable Binding Site Detection and Descriptor Calculation with DoGSite3. J Chem Inf Model. 2023;63(10):3128-3137.

19. Sato Y, Ramalanjaona N, Huet T, et al. The "Phantom Effect" of the Rexinoid LG100754: structural and functional insights. PLoS One. 2010;5(11):e15119.

20. Morris GM, Huey R, Lindstrom W, et al. AutoDock4 and AutoDockTools4: Automated docking with selective receptor flexibility. J Comput Chem. 2009;30(16):2785-2791.

21. Hanwell MD, Curtis DE, Lonie DC, et al. Avogadro: an advanced semantic chemical editor, visualization, and analysis platform. J Cheminform. 2012;4(1):17.

22. Chen J, Liu H, Wang F, et al. Relapse Analysis and Resistance Mutations of PML::RARA Fusion Gene in Acute Promyelocytic Leukemia Patients Treated with All-Trans Retinoic Acid and Arsenic (Poster-ASH meeting). Blood. 2021;138:2243–2245.

23. Zhu HH, Qin YZ, Huang XJ. Resistance to arsenic therapy in acute promyelocytic leukemia. N Engl J Med. 2014;370(19):1864-1866.

24. Gallagher RE, Moser BK, Racevskis J, et al. Treatment-influenced associations of PML::RARAlpha mutations, FLT3 mutations, and additional chromosome abnormalities in relapsed acute promyelocytic leukemia. Blood. 2012;120(10):2098-2108.

25. Hattori H, Ishikawa Y, Kawashima N, et al. Identification of the novel deletion-type PML::RARA mutation associated with the retinoic acid resistance in acute promyelocytic leukemia. PLoS One. 2018;13(10):e0204850.

26. Lou Y, Ma Y, Sun J, et al. Evaluating frequency of PML::RARA mutations and conferring resistance to arsenic trioxide-based therapy in relapsed acute promyelocytic leukemia patients. Ann Hematol. 2015;94(11):1829-1837.

27. Iaccarino L, Ottone T, Alfonso V, et al. Mutational landscape of patients with acute promyelocytic leukemia at diagnosis and relapse. Am J Hematol. 2019;94(10):1091-1097.

28. Iaccarino L, Ottone T, Divona M, et al. Mutations affecting both the rearranged and the unrearranged PML alleles in refractory acute promyelocytic leukaemia. Br J Haematol. 2016;172(6):909-913.

29. Marasca R, Zucchini P, Galimberti S, et al. Missense mutations in the PML::RARAlpha ligand binding domain in ATRA-resistant As(2)O(3) sensitive relapsed acute promyelocytic leukemia. Haematologica. 1999;84(11):963-968.

30. Gallagher RE, Schachter-Tokarz EL, Zhou DC, et al. Relapse of acute promyelocytic leukemia with PML::RARAlpha mutant subclones independent of proximate all-trans retinoic acid selection pressure. Leukemia. 2006;20(4):556-62.

31. Ding W, Li YP, Nobile LM, et al. Leukemic cellular retinoic acid resistance and missense mutations in the PML::RARAlpha fusion gene after relapse of acute promyelocytic leukemia from treatment with all-trans retinoic acid and intensive chemotherapy. Blood. 1998;92(4):1172-1183.